Extrapolation of D^* meson cross section measured in CMS at 7 TeV together with the total charm cross section

Max Uetrecht[1]

supervised by: Dr. Achim Geiser[2] & Yewon Yang[2]

[1]TU Dortmund University
max.uetrecht@udo.edu

[2]DESY Hamburg CMS Group
{achim.geiser, yewon.yang}@desy.de

DESY Summer Student Program, 2022
Period: July 19 - September 08

Abstract

The goal of the summer student project was to extrapolate the D^* meson cross section measured in the CMS experiment at $\sqrt{s} = 7$ TeV by applying the Fixed Order plus Next-to-Leading logarithms (FONLL) scheme, a theoretical perturbative expansion of a QCD cross section. Taking into account the most recent charm-hadron fragmentation fraction measurements from ALICE, we applied a p_T-dependent correction to the c-hadron fractions and thus moved away from their assumed collision-system- and p_T-independence.
As a basic reference of our extrapolation strategy, we extrapolated first ALICE, CMS and LHCb data of D^0 meson production at 5 TeV and determined ranges of initial parameters to vary around for 7 TeV D^* meson data measured in CMS and LHCb.
Furthermore, we checked and compared applying a p_T-dependent correction to the c-hadron fractions with previous results, where universality (in a sense that fractions are collision-system- and p_T-independent) has been assumed.

Contents

1 Introduction

Our goal is to extrapolate the D^* meson cross section measured in the CMS detector in the LHC at $\sqrt{s} = 7\,\text{TeV}$ to extract the total charm quark production cross section.
Experimentally, a double differential cross section with respect to the rapidity y and transverse momentum p_T has been measured by the CMS experiment. Since CMS only provided measurements for $p_T > 1$ GeV and $0 < y < 2.5$, we seek to extrapolate (or respectively interpolate) the measurements to the full phase space of y and p_T and determine the total cross section on the full phase space. While technically the full phase space is only constrained by kinematics, we restrict ourselves to $0 < p_T < 300$ GeV and $0 < y < 8.5$ (we synonymously refer to these upper boundaries of y and p_T as ∞), assuming most of the total cross section lies within this phase space.

According to the *factorization theorem*[1] of QCD, p_T-differential cross sections $\frac{\mathrm{d}\sigma(pp\to X)}{\mathrm{d}p_T}$ of pp collisions to a hadronic final state X (containing charm quarks) are computed as the convolution of

1. the parton distribution functions (PDF) $f_i(x, \mu_f^2)$, specifying the probability density of finding a parton with longitudinal momentum fraction x at a scale μ_f^2,
2. the partonic cross section $\hat{\sigma}(q_i q_j \to c\bar{c})$, where q_i and q_j initial states are given by $gg, q\bar{q}$ or qg with q being a light quark and g being a gluon,
3. the non-perturbative fragmentation function, describing the hadronization of quarks into hadrons.

After having calculated the charm-quark (c-quark) production cross section and having applied the fragmentation function to it, we apply a c-hadron fragmentation fraction $f(c \to X)$ indicating the percentage of c-quarks hadronizing into X so that we obtain the cross section $\sigma(pp \to X)$.

In the past, empirical data suggested a collision system and p_T-independence of c-quark hadronization. The recent ALICE publication [2] provided evidence to the contrary, indicating that the c-hadron fractions are indeed p_T- and collision-system-dependent (e.g. pp collision). Thus we will employ the results from [2] to derive a p_T-dependent correction to $f(c \to X)$, which in total we will call *p_T-dependent c-hadron fractions.* A proper reference for the derivation of the p_T-dependent correction will be provided by the supervisors after this summer student project.

For this study, we make use of the theoretical Fixed Order plus Next-to-Leading logarithms (FONLL) scheme[3], a perturbative expansion of the QCD c-quark production cross section, in which divergent logarithms are controlled by resummation techniques, and the non-perturbative Kartvelishvili function[4] for fragmentation of c-quarks into hadrons.
Our theoretical framework gives us three free parameters we can consider in this study: the Kartvelishvili parameter α as well as the renormalization and factorization scales $\mu_{r,f}$, which we introduce to be defined as

$$\mu_{r,f} \equiv 2^{x_{r,f}} \times \mu_0 \tag{1}$$

with $\mu_0 = \sqrt{m_c^2 + p_T^2}$, where $m_c = 1.5\,\text{GeV}$ is the c-quark pole mass and p_T denotes its transverse momentum. All three free parameters will be determined by the FONLL predictions with the lowest χ^2 value[5] to the data.

In order to acquire FONLL predictions, we use the fortran tool FONLL[6] in combination with the *CTEQ6.6* parton distribution function (PDF). Concretely, we use the FONLL tool to calculate differential cross sections $\frac{\mathrm{d}\sigma(pp\to X)}{\mathrm{d}p_T}$ or $\frac{\mathrm{d}\sigma(pp\to X)}{\mathrm{d}y}$ for charm quark production and then apply the charm-quark fragmentation function to obtain the differential production cross section for the respective meson X.

2 Extrapolation of D^0 meson cross section measured at 5 TeV in LHC

Since neither CMS or LHCb provides measurements for the D^* meson cross section at 7 TeV in the $0 < p_T < 1$ GeV bin for all values of the rapidity y[1], in which a large percentage of the total cross section lies, we first want to find suitable parameters for the scales $\mu_{r,f}$ and the Kartvelishvili parameter α by studying $\frac{D^0+\overline{D^0}}{2}$ meson production at $\sqrt{s} = 5\,\text{TeV}$. Fortunately, data measured in the ALICE, CMS and LHCb detector covers the whole phase space from $0 < p_T < 6$ GeV and $0 < y < 4.5$ and thus allows us to look at p_T- or y-integrated single-differential cross sections $\frac{d\sigma}{dy}$ or $\frac{d\sigma}{dp_T}$.
We furthermore want to study the consistency of our data with both p_T-dependent and p_T-independent c-hadron fractions.

A similar study has already been done in 2021 (see [7]) using ALICE, CMS and LHCb data at 5 TeV to extrapolate $\frac{D^0+\overline{D^0}}{2}$ cross section and the total c-quark production cross section, assuming *p_T- and collision-system-independent* c-hadron fractions by using the average value, measured in e^+e^- collisions around 10.5 GeV with $X = D^0$ ($f(c \to D^0)^{e^+e^-,\text{ average}} = 0.577$, see [8]). Contrary to the study from 2021, we use the most recent $X = D^0$ fraction measured from pp collision at ALICE (i.e. $f(c \to D^0) = 39.1 \pm 1.7(\text{ stat })^{+2.5}_{-3.7}(\text{ syst })$ in percent, see [2]) and differentiate between applying the aforementioned p_T-dependent correction or not.

An overview of the used measurements, together with their kinematic ranges for the rapidity y and the transverse momentum p_T is given in Table 1. Henceforth we will call the common kinematic ranges of all measurements the common phase space, on which we will conduct our research ($0 < p_T < 6$ GeV and $0 < y < 4.5$).
In the following, we will first create a suitable grid for acquiring FONLL predictions on the phase space and then discuss the undertaken steps of finding the best parameters for the given data. This will allow us to obtain FONLL predictions for the total c-quark production cross section, which should - within uncertainties, which are to be determined later - already be close to the final extrapolated total cross section.

Experiment	y range	p_T range	Reference
ALICE	$\lvert y\rvert < 0.5$	$0 < p_T < 36$ GeV	[9]
CMS	$\lvert y\rvert < 1.0$	$2 < p_T < 100$ GeV	[10]
LHCb	$2.0 < y < 2.5$	$0 < p_T < 10$ GeV	[11]
	$2.5 < y < 3.0$	$0 < p_T < 10$ GeV	
	$3.0 < y < 3.5$	$0 < p_T < 10$ GeV	
	$3.5 < y < 4.0$	$0 < p_T < 9$ GeV	
	$4.0 < y < 4.5$	$0 < p_T < 6$ GeV	

Table 1: Used measurements for differential production cross sections of D^0 mesons at $\sqrt{s} = 5$ TeV pp-collision and their kinematic ranges for the rapidity y and transverse momentum p_T.

2.1 Construction of a suitable grid for the phase space

Like in all numerical calculations, we have to discretize the underlying phase space, as we cannot directly compute differential quantities with FONLL. To compute quantities with FONLL, we first have to create a suitable grid covering all of our phase space ($0 < p_T < 300$ GeV and $0 < y < 8.5$). The grid creation process of FONLL requires input for the center of mass energy, the used PDF, the quark mass, the renormalization and fragmentation scales $\mu_{r,f}$ and binning for y and p_T.

Since the FONLL web tool http://www.lpthe.jussieu.fr/ cacciari/fonll/fonllform.html already generates expected results within our phase space, we obtained results for the differential cross section $\frac{\mathrm{d}\sigma(pp\to D^*)}{\mathrm{d}p_T}$ with y integrated from $-1.0 < y < 1.0$ in p_T bins of width 1 GeV from 0 GeV to 10 GeV from the web tool. After that, we computed the same differential cross section with the FONLL script and a grid with binning we chose.

[1] LHCb provides measurements for $0 < p_T < 1$ GeV only in some rapidity bins, see Table 1.

Our goal was to tune the grid so that our predictions match the ones from the web as best as possible. In the end, we achieved a relative error of 0.161% and thus used our choice of grid bins for y and p_T for all further calculations.

2.2 Determining renormalization and factorization scales

At first, we want to determine the renormalization and factorization scales x_r and x_f suitable to describe our data. For this, we start with the common phase space and study the y-differential cross section $\frac{d\sigma}{dy}$, where the FONLL predictions do not depend on the specific value of the Kartvelishvili fragmentation parameter α.
With regards to data, we only use p_T-integrated values from ALICE and LHCb (see Table 1) since the CMS measurement does not cover the whole p_T phase space up to 6 GeV. Thus we only have to vary the scales when finding suitable parameters to describe our data with FONLL predictions.
To find suitable scales, we varied x_r between 0 and -1.25 while fixing $x_f \in \{0, 0.25, 0.5, 0.75, 1.0\}$. In short notation, we always refer to the used scales (or scale sets) as a two-tuple (x_f, x_r).
Given our six y-bins of data and one free parameter to determine (the scale x_r), we use a χ^2 test[5] and thus seek to minimize

$$\chi^2 \equiv \sum_{y \text{ bins}} \frac{(\text{ FONLL } - \text{ data })^2}{\text{statistic error }^2 + \text{ systematic error }^2}. \tag{2}$$

The FONLL predictions for the differential cross section $\frac{d\sigma}{dy}$ for every fixed value of x_f, together with the χ^2 values of all probed scales can be found in the following plots.
As a result, the best scales for each value of x_f can be found in Table 2.

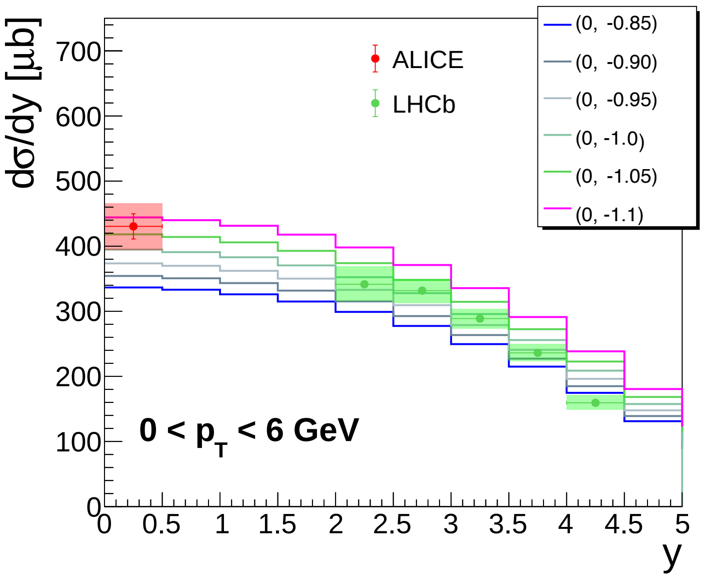

Figure 2: FONLL predictions for $\frac{d\sigma}{dy}$ together with ALICE and LHCb data of D^0 meson cross section (see Table 1) for different scales x_r, while keeping x_f fixed (scales two-tuple: $(x_f = 0.0,\, x_r)$).

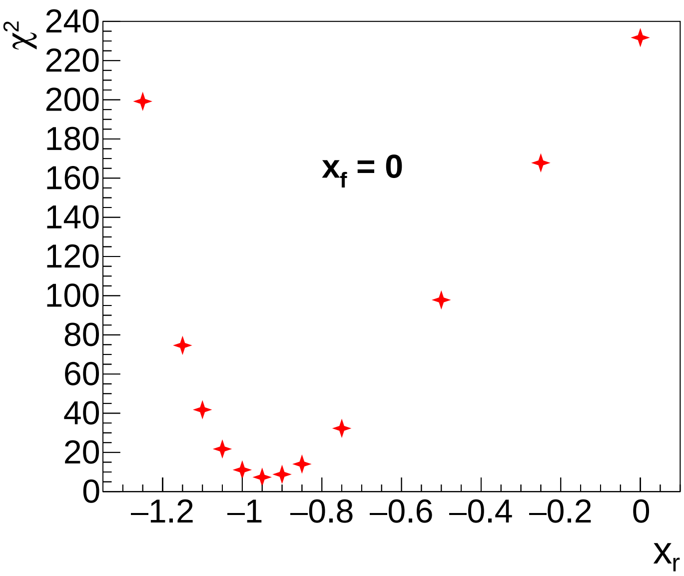

Figure 3: χ^2 test on FONLL predictions and actual data for all probed scales x_r while keeping x_f fixed. The best scale turned out to be $x_r = -0.95$.

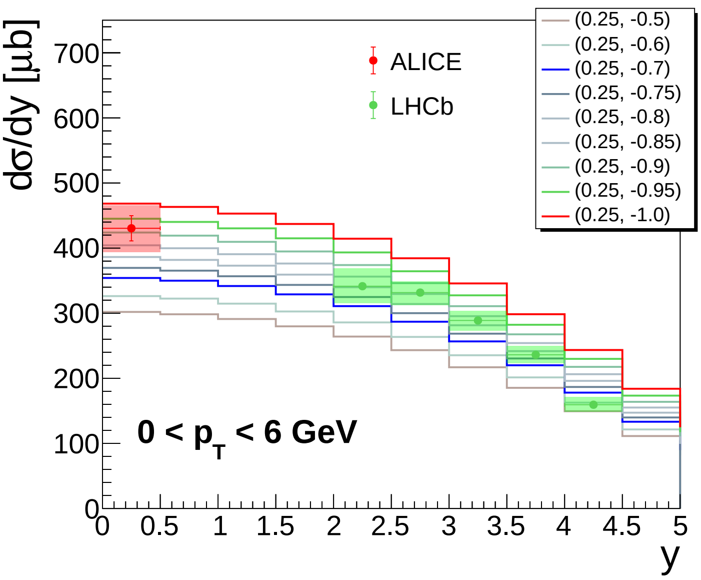

Figure 4: FONLL predictions for $\frac{d\sigma}{dy}$ together with ALICE and LHCb data of D^0 meson cross section (see Table 1) for different scales x_r, while keeping x_f fixed (scales two-tuple: $(x_f = 0.25,\, x_r)$).

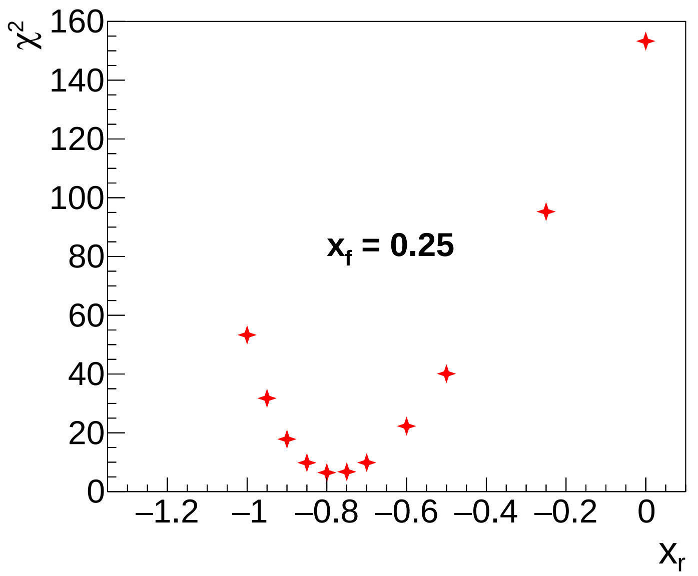

Figure 5: χ^2 test on FONLL predictions and actual data for all probed scales x_r while keeping x_f fixed. The best scale turned out to be $x_r = -0.8$.

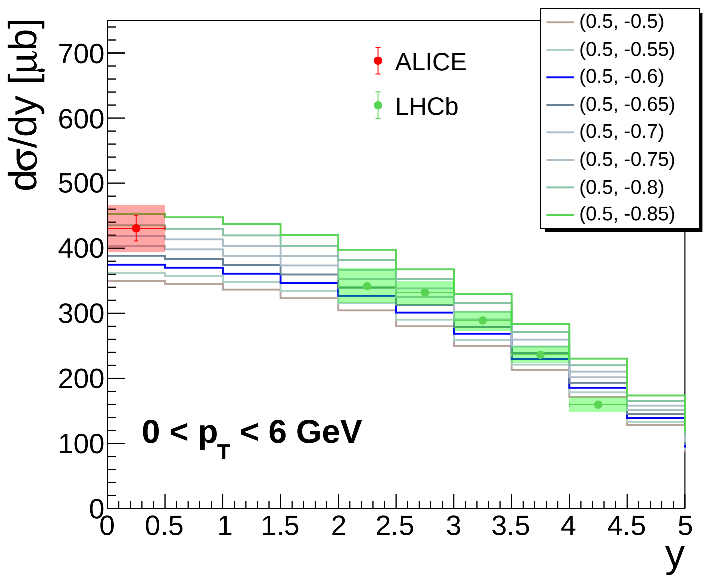

Figure 6: FONLL predictions for $\frac{d\sigma}{dy}$ together with ALICE and LHCb data of D^0 meson cross section (see Table 1) for different scales x_r, while keeping x_f fixed (scales two-tuple: ($x_f = 0.5$, x_r)).

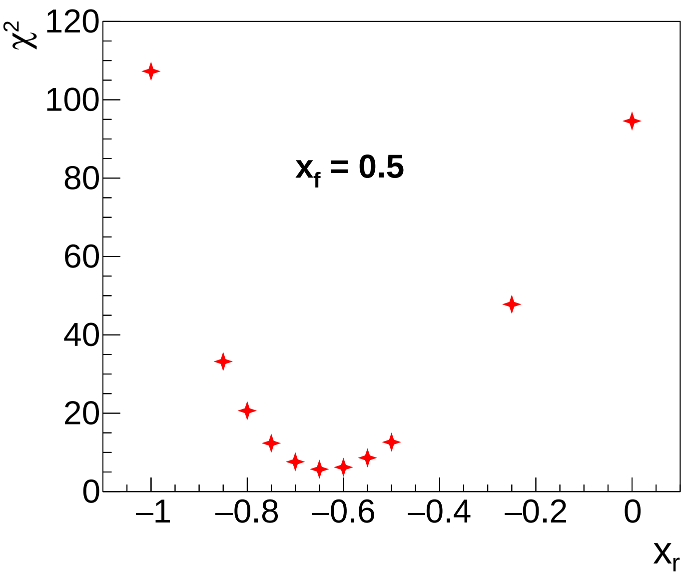

Figure 7: χ^2 test on FONLL predictions and actual data for all probed scales x_r while keeping x_f fixed. The best scale turned out to be $x_r = -0.65$.

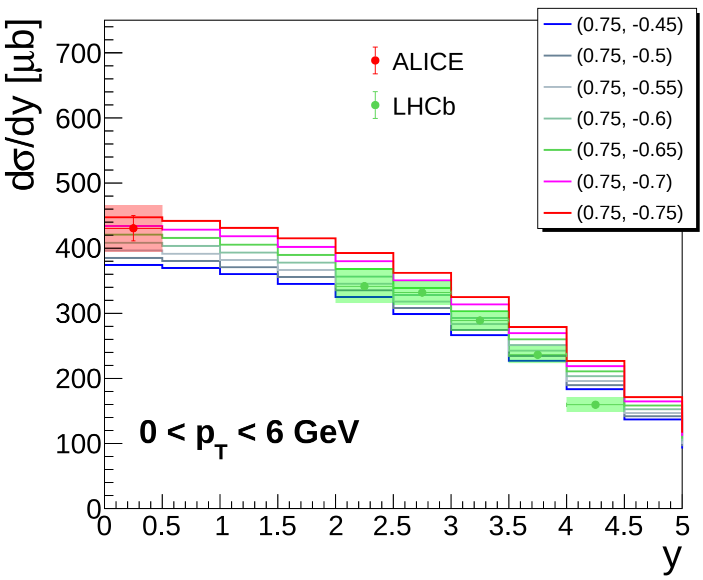

Figure 8: FONLL predictions for $\frac{d\sigma}{dy}$ together with ALICE and LHCb data of D^0 meson cross section (see Table 1) for different scales x_r, while keeping x_f fixed (scales two-tuple: ($x_f = 0.75$, x_r)).

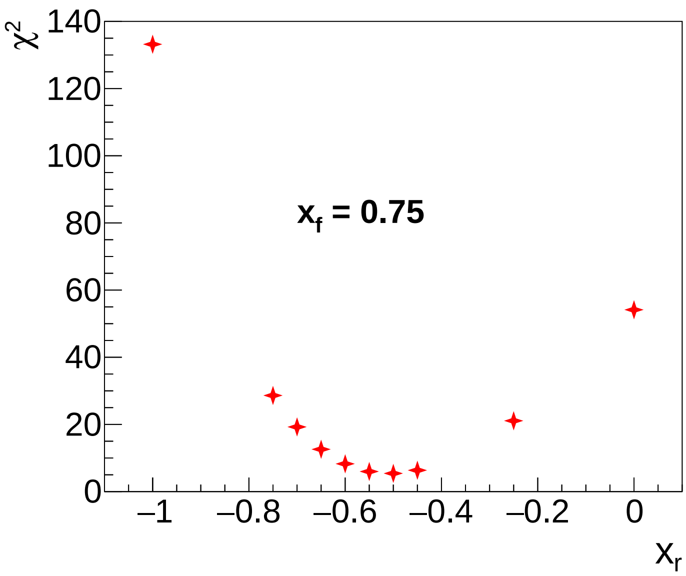

Figure 9: χ^2 test on FONLL predictions and actual data for all probed scales x_r while keeping x_f fixed. The best scale turned out to be $x_r = -0.5$

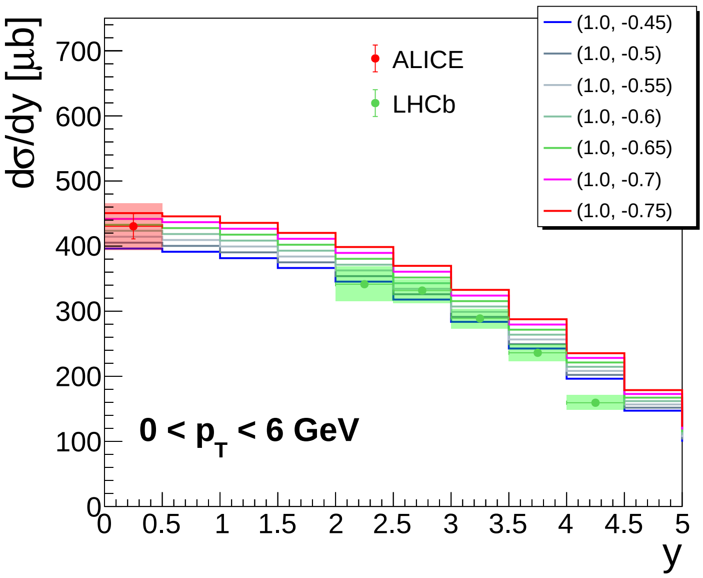

Figure 10: FONLL predictions for $\frac{d\sigma}{dy}$ together with ALICE and LHCb data of D^0 meson cross section (see Table 1) for different scales x_r, while keeping x_f fixed (scales two-tuple: $(x_f = 1.0,\, x_r)$).

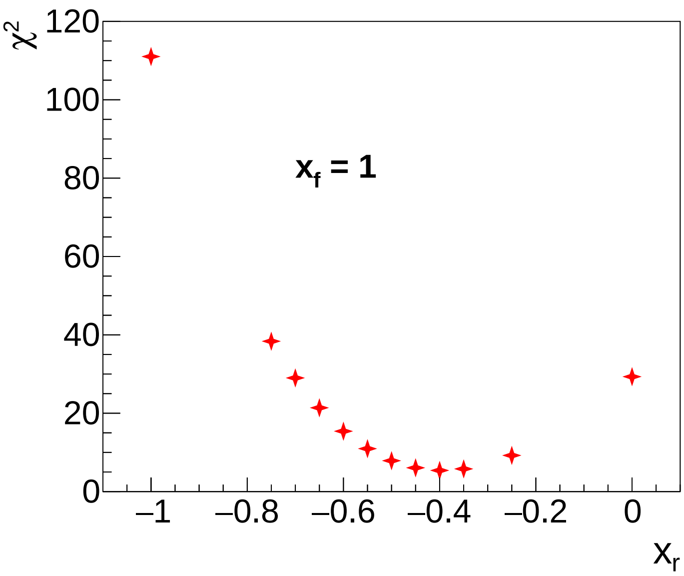

Figure 11: χ^2 test on FONLL predictions and actual data for all probed scales x_r while keeping x_f fixed. The best scale turned out to be $x_r = -0.4$

2.2.1 Summarizing the best scale sets obtained from y-distributions

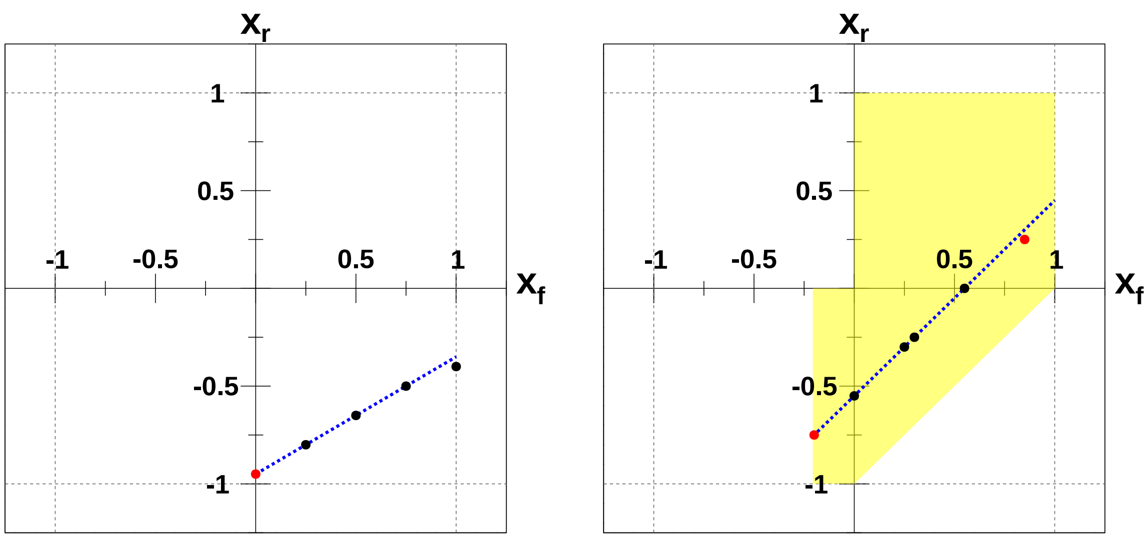

Figure 12: Best five scale sets describing y-distributions of 5 TeV D^0 meson production by χ^2 value together with an interpolation line. Left: Results for this study. Right: Results from the 2021 study[7]

Summarizing our results, the best scale sets and their corresponding χ^2 value can be found in Table 2 (scale sets plotted in Figure 12). Comparing our results to the extrapolation study from 2021[7], where a p_T-independent c-hadron fraction, averaged from e^+e^--collision at 10.5 GeV has been used $(f(c \to D^0)^{e^+e^-,average} = 0.577$, see [8]), we only focus on the common scale set having $x_f = 0$.
In our case, this scale set turned out to be $(0, -0.95)$ with $\chi^2 = 7.34512$; in the previous study $(0, -0.55)$ with $\chi^2 = 5.0173$.

In order to qualitatively explain the different slope of the interpolation line, we consider Figure 13: Shown are two y-distributions, together with FONLL predictions varying x_f and x_r while keeping the other value fixed, for a p_T-integrated differential cross section from the 2021 study.
It should be noted that variations in the renormalization scale x_r has a larger effect when the value

itself decreases (left plot), whereas the factorization scale x_f is a bit more sensitive to variations when it decreases itself (right plot). Therefore we can expect that the slope of our results to be lower than the one of 2021, which indicates the renormalization scale having a larger effect than the factorization in our results.

χ^2	Best scale sets (x_f, x_r)
7.34512	$(0, -0.95)$
6.46289	$(0.25, -0.8)$
5.71467	$(0.5, -0.65)$
5.41831	$(0.75, -0.5)$
5.40474	$(1.0, -0.4)$

Table 2: Result of the χ^2-test with $f = 5$ d.o.f. on rapidity bins using p_T-integrated differential cross sections from ALICE and LHCb (see Table 1).

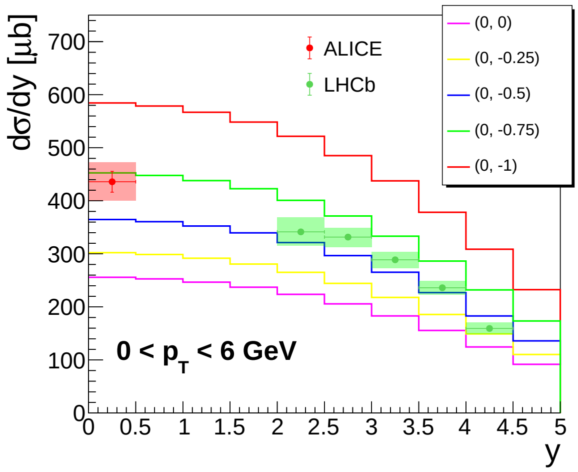

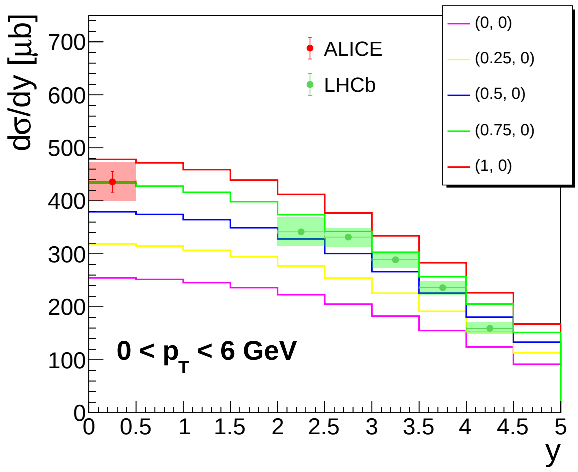

Figure 13: FONLL predictions varying x_f and x_r (two-tuple notation: (x_f, x_r)) while keeping the other value fixed for the p_T-integrated differential D^0 meson cross section $\frac{d\sigma}{dy}$, together with ALICE and LHCb data of 5 TeV D^0 meson production, taken from the 2021 study [7].

2.3 Determining α of the Kartvelishvili fragmentation function

After we have determined five scale sets (see Table 2) that describe the y-bins of the differential cross section $\frac{d\sigma}{dy}$ best, we will determine the Kartvelishvili fragmentation parameter α by looking at the $\frac{d\sigma}{dp_T}$ distribution of our data. Since our c-hadron fractions are not y but p_T dependent (for p_T-independent c-hadron fractions applied on p_T-distributions see subsection 5.1), we only have to vary α around our five best scales. To determine a suitable α describing our data, we vary it in steps of one between 6 and 15.

In the following we show p_T-distribution plots and χ^2 curves for ALICE, CMS and LHCb in the order of the five scale sets in Table 2.

2.3.1 ALICE

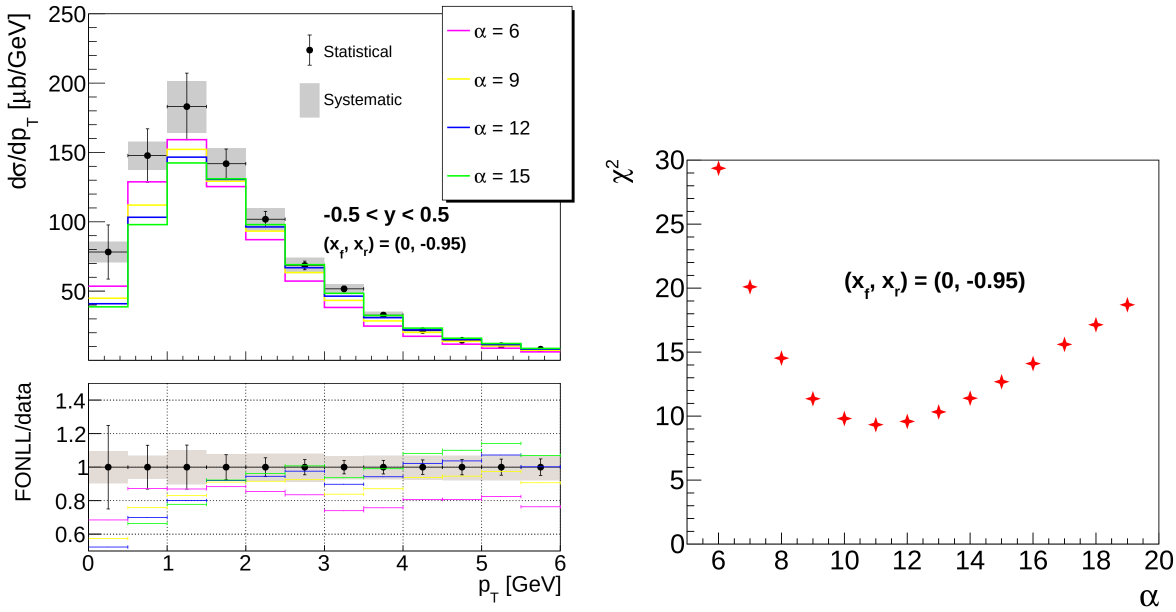

Figure 14: FONLL predictions with p_T-dependent c-hadron fractions and χ^2-test values with $f = 11$ d.o.f. for $\frac{d\sigma}{dp_T}$ together with ALICE data for different values of α.

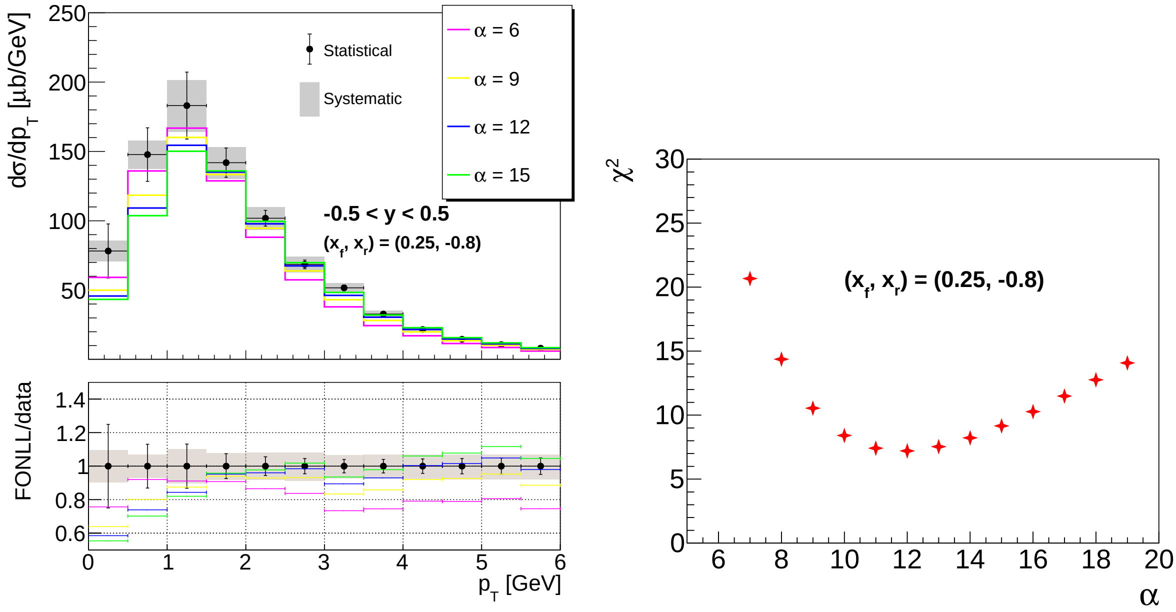

Figure 15: FONLL predictions with p_T-dependent c-hadron fractions and χ^2-test values with $f = 11$ d.o.f. for $\frac{d\sigma}{dp_T}$ together with ALICE data for different values of α.

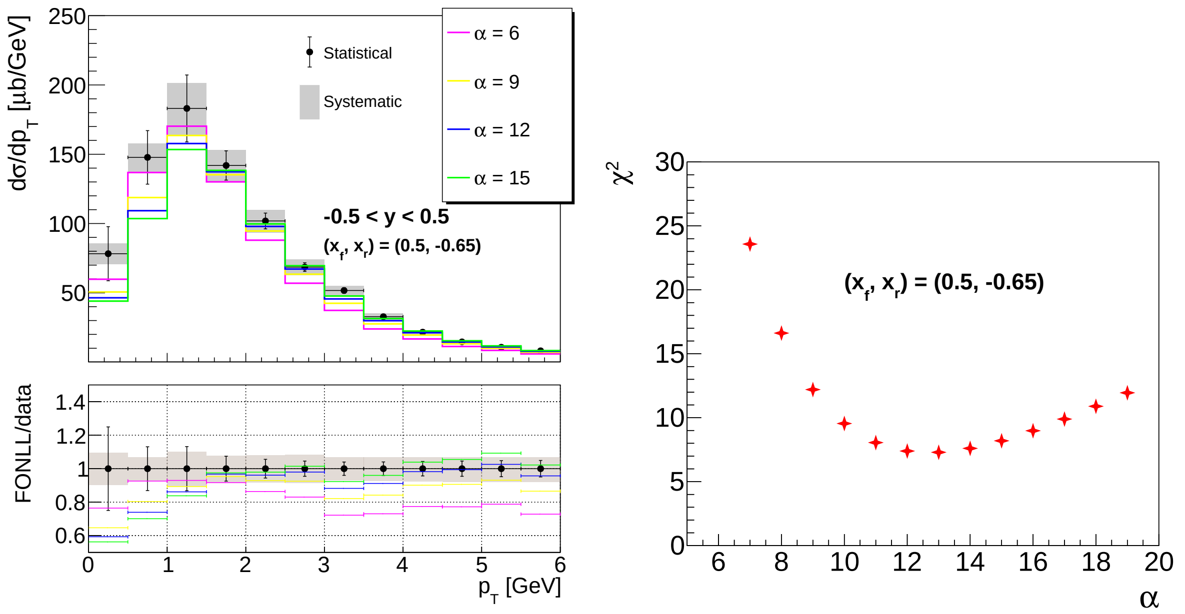

Figure 16: FONLL predictions with p_T-dependent c-hadron fractions and χ^2-test values with $f = 11$ d.o.f. for $\frac{d\sigma}{dp_T}$ together with ALICE data for different values of α.

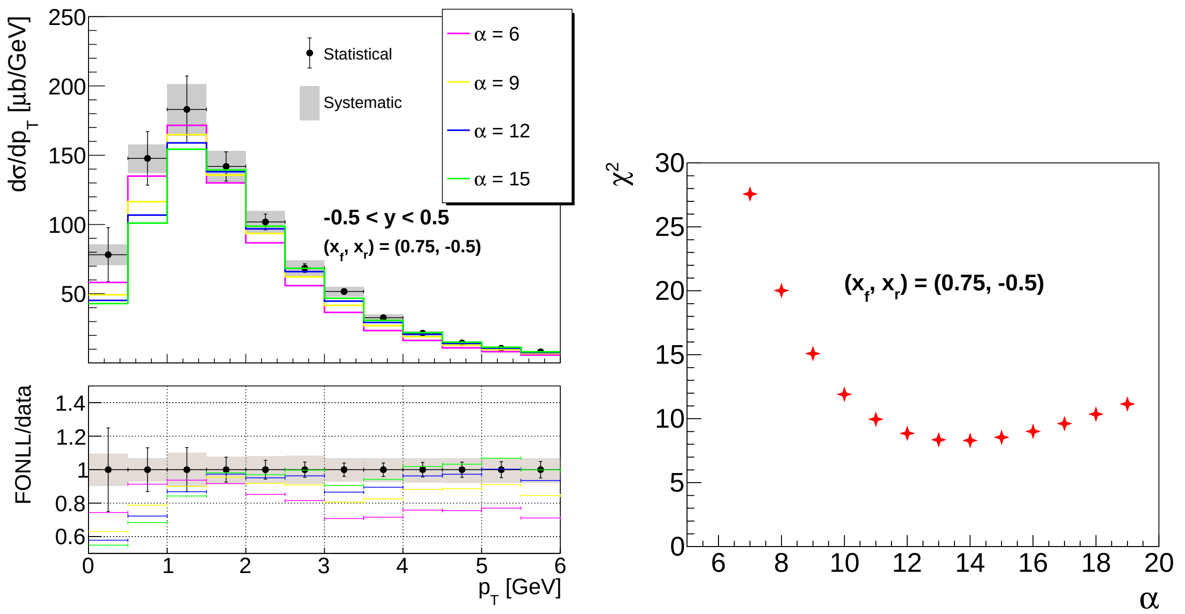

Figure 17: FONLL predictions with p_T-dependent c-hadron fractions and χ^2-test values with $f = 11$ d.o.f. for $\frac{d\sigma}{dp_T}$ together with ALICE data for different values of α.

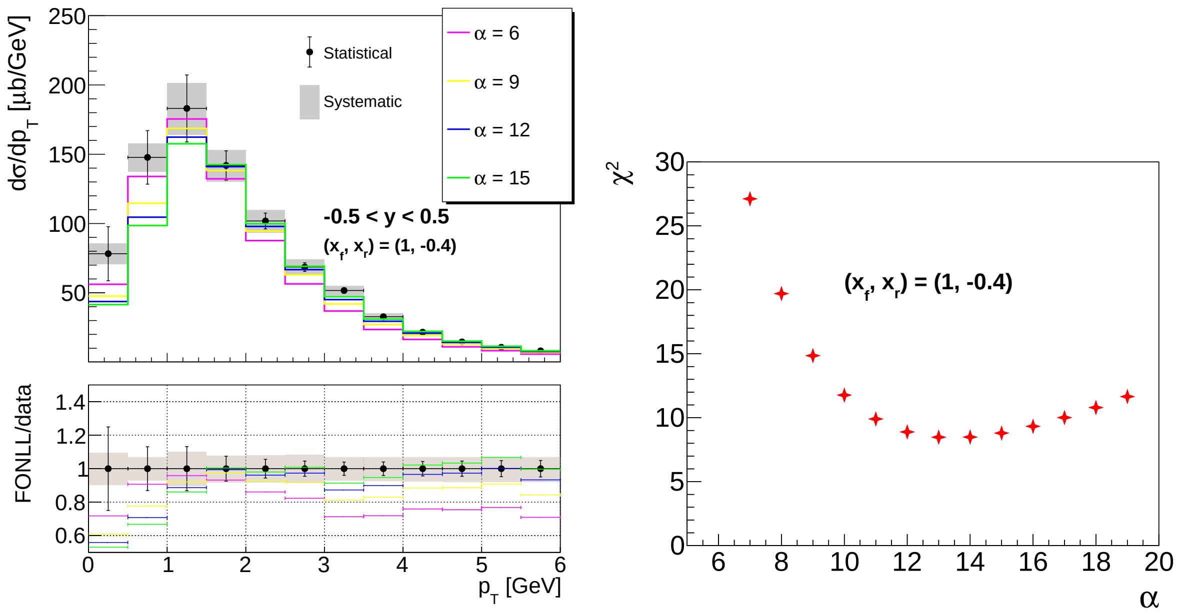

Figure 18: FONLL predictions with p_T-dependent c-hadron fractions and χ^2-test values with $f = 11$ d.o.f. for $\frac{d\sigma}{dp_T}$ together with ALICE data for different values of α.

2.3.2 CMS

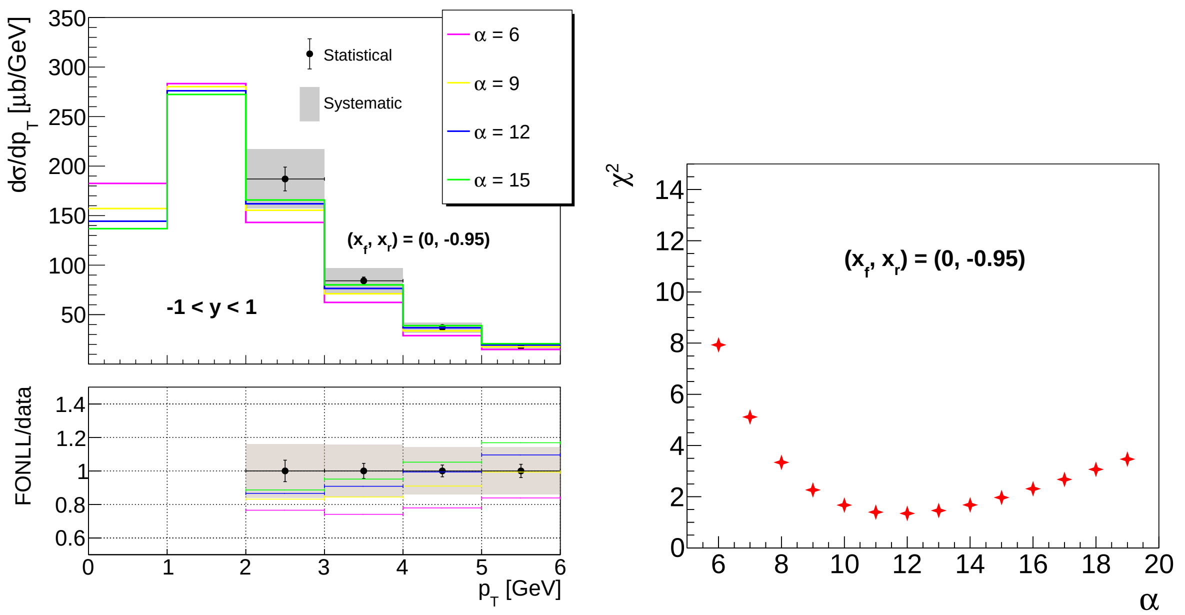

Figure 19: FONLL predictions with p_T-dependent c-hadron fractions and χ^2-test values with $f = 3$ d.o.f. for $\frac{d\sigma}{dp_T}$ together with CMS data for different values of α.

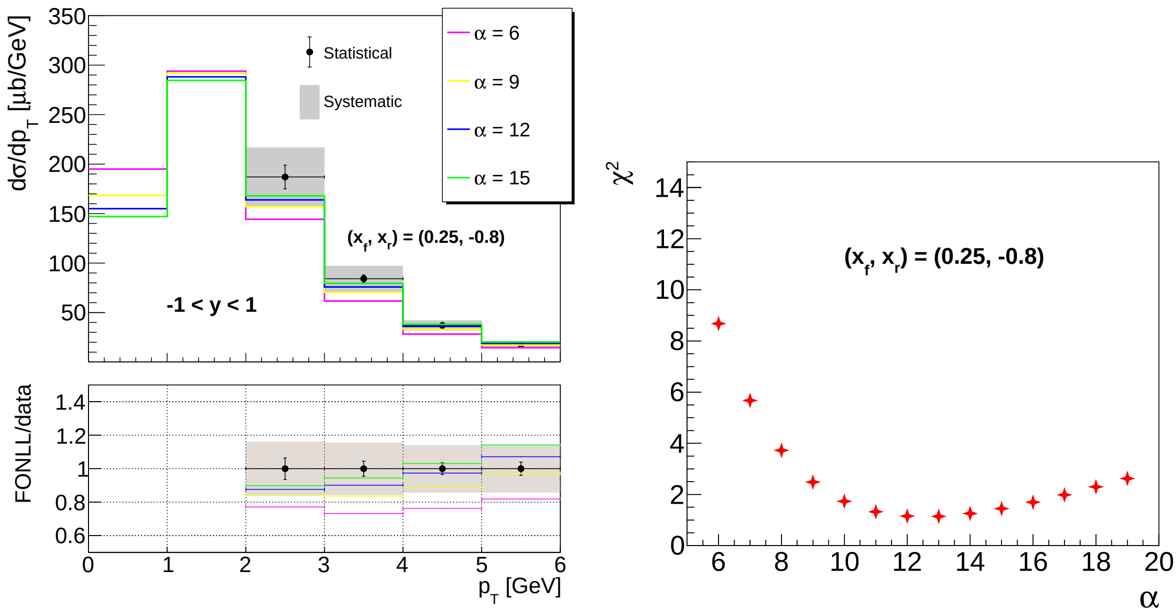

Figure 20: FONLL predictions with p_T-dependent c-hadron fractions and χ^2-test values with $f = 3$ d.o.f. for $\frac{d\sigma}{dp_T}$ together with CMS data for different values of α.

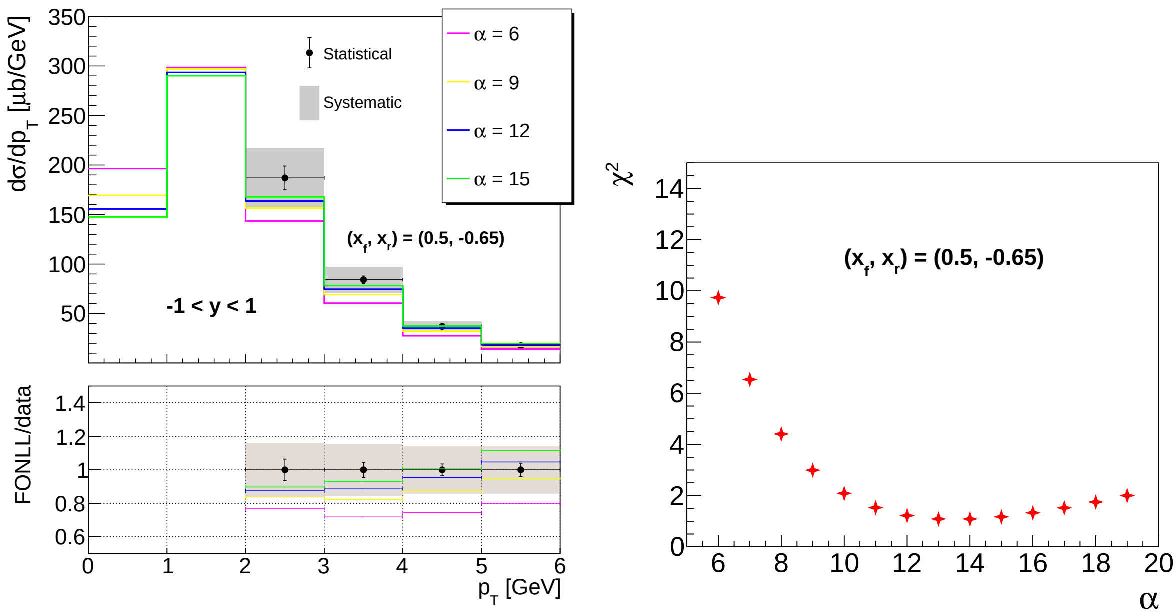

Figure 21: FONLL predictions with p_T-dependent c-hadron fractions and χ^2-test values with $f = 3$ d.o.f. for $\frac{d\sigma}{dp_T}$ together with CMS data for different values of α.

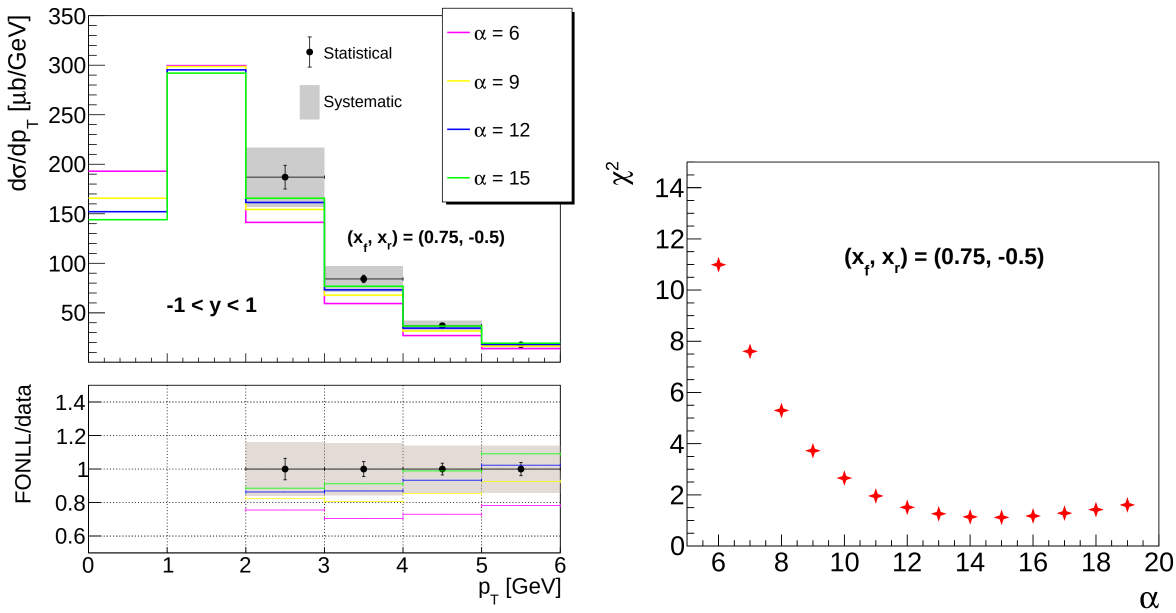

Figure 22: FONLL predictions with p_T-dependent c-hadron fractions and χ^2-test values with $f = 3$ d.o.f. for $\frac{d\sigma}{dp_T}$ together with CMS data for different values of α.

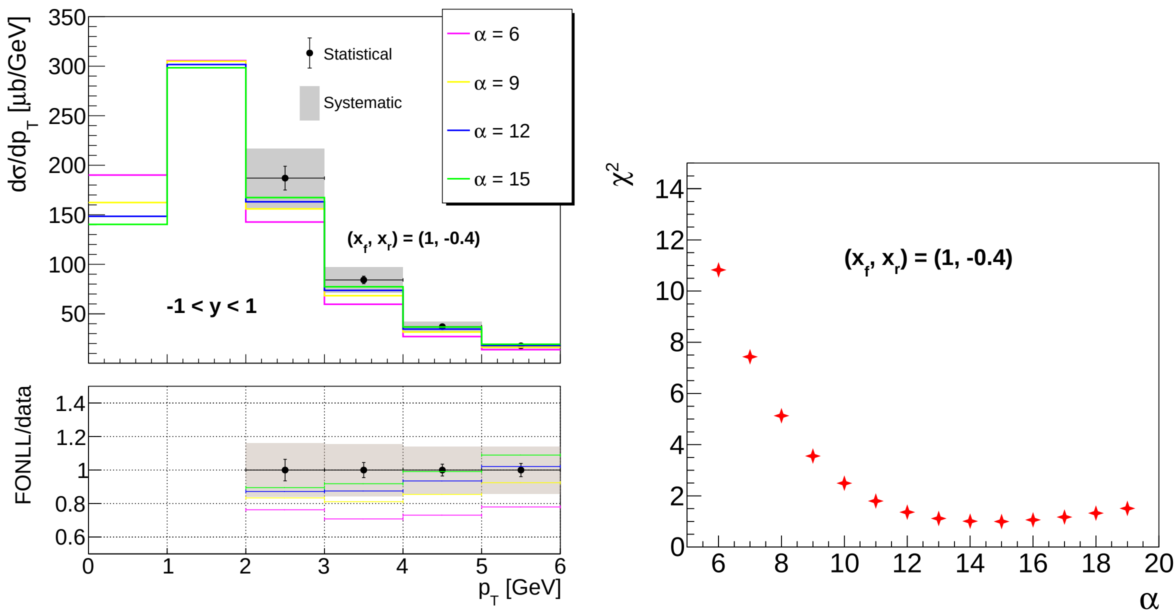

Figure 23: FONLL predictions with p_T-dependent c-hadron fractions and χ^2-test values with $f = 3$ d.o.f. for $\frac{d\sigma}{dp_T}$ together with CMS data for different values of α.

2.3.3 LHCb

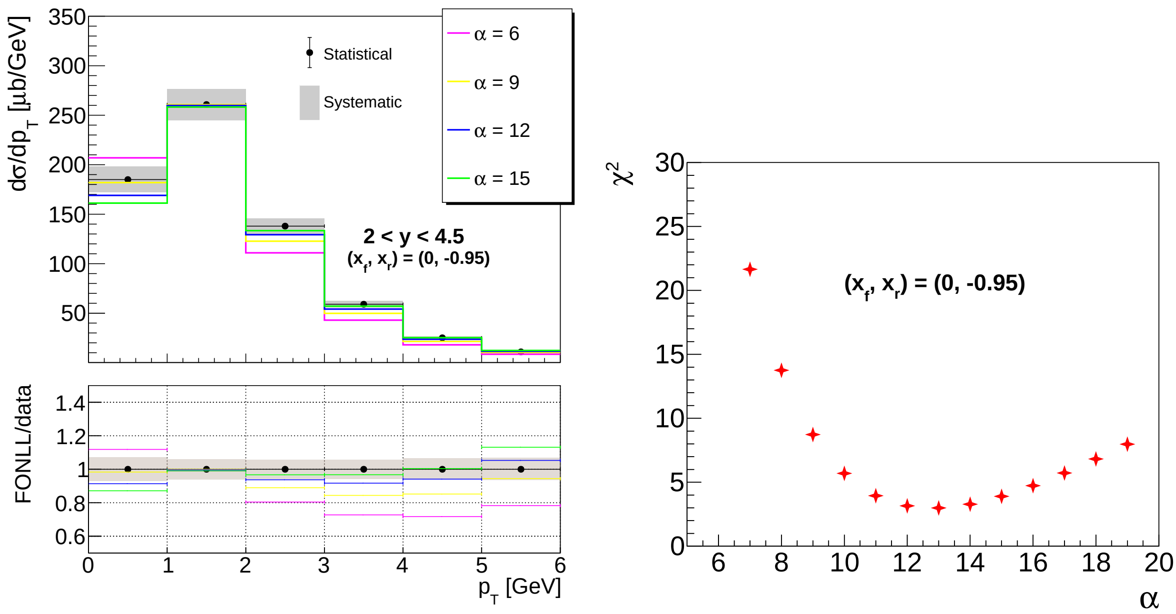

Figure 24: FONLL predictions with p_T-dependent c-hadron fractions and χ^2-test values with $f = 5$ d.o.f. for $\frac{d\sigma}{dp_T}$ together with LHCb data for different values of α.

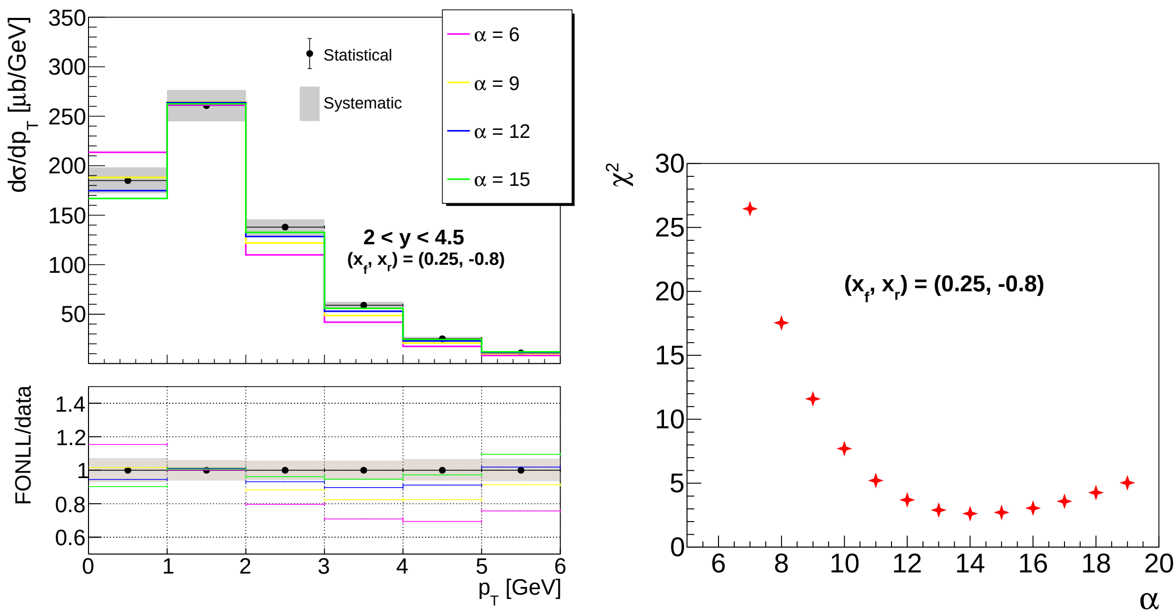

Figure 25: FONLL predictions with p_T-dependent c-hadron fractions and χ^2-test values with $f = 5$ d.o.f. for $\frac{d\sigma}{dp_T}$ together with LHCb data for different values of α.

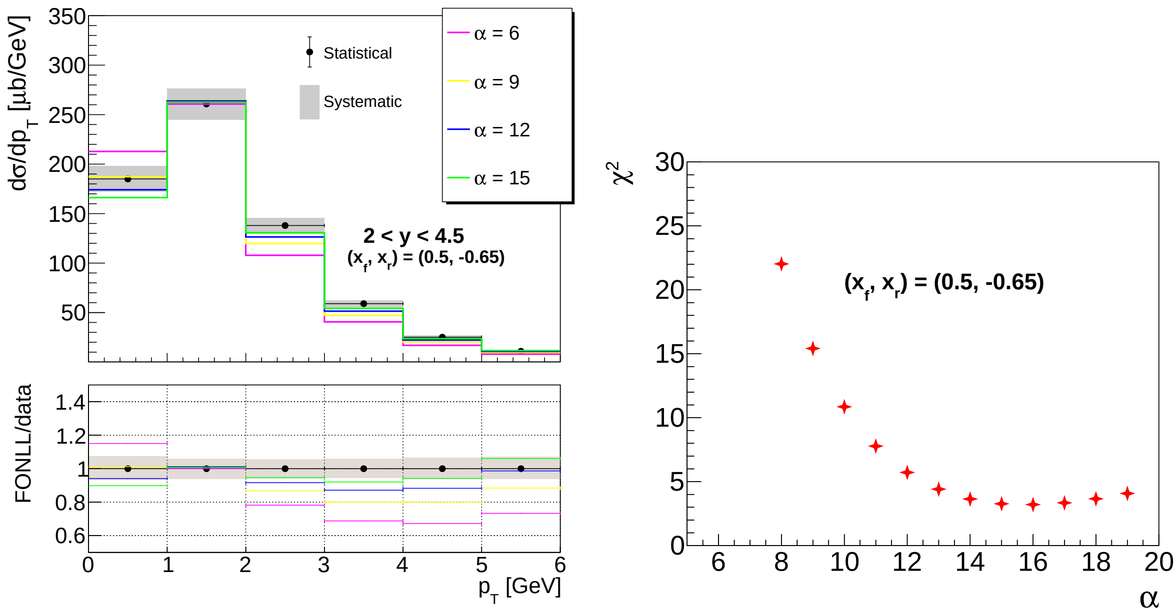

Figure 26: FONLL predictions with p_T-dependent c-hadron fractions and χ^2-test values with $f = 5$ d.o.f. for $\frac{d\sigma}{dp_T}$ together with LHCb data for different values of α.

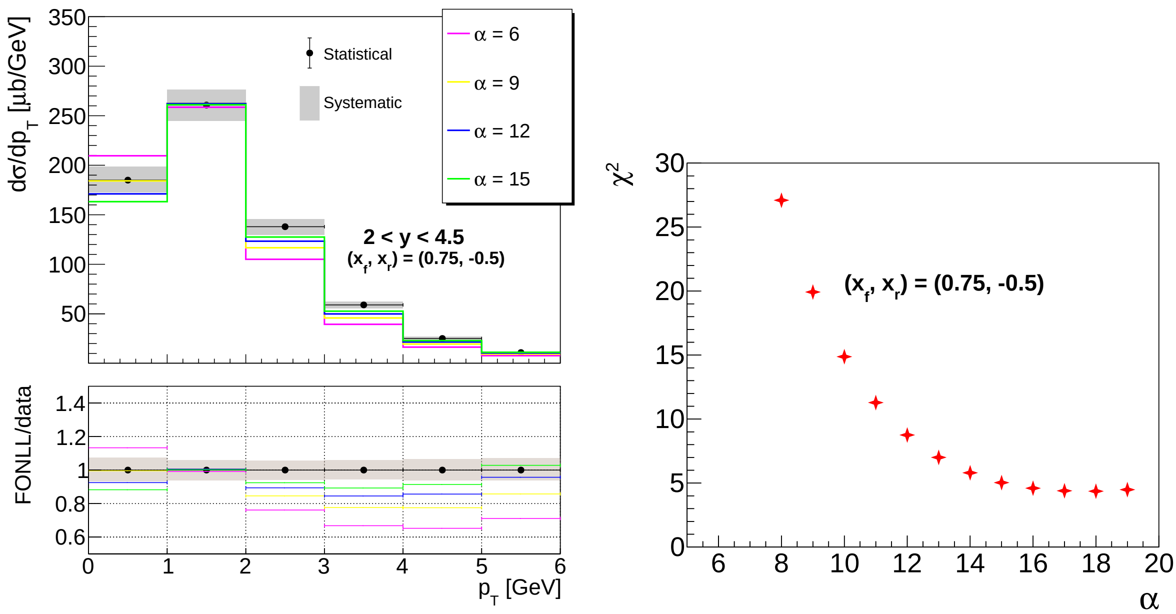

Figure 27: FONLL predictions with p_T-dependent c-hadron fractions and χ^2-test values with $f = 5$ d.o.f. for $\frac{d\sigma}{dp_T}$ together with LHCb data for different values of α.

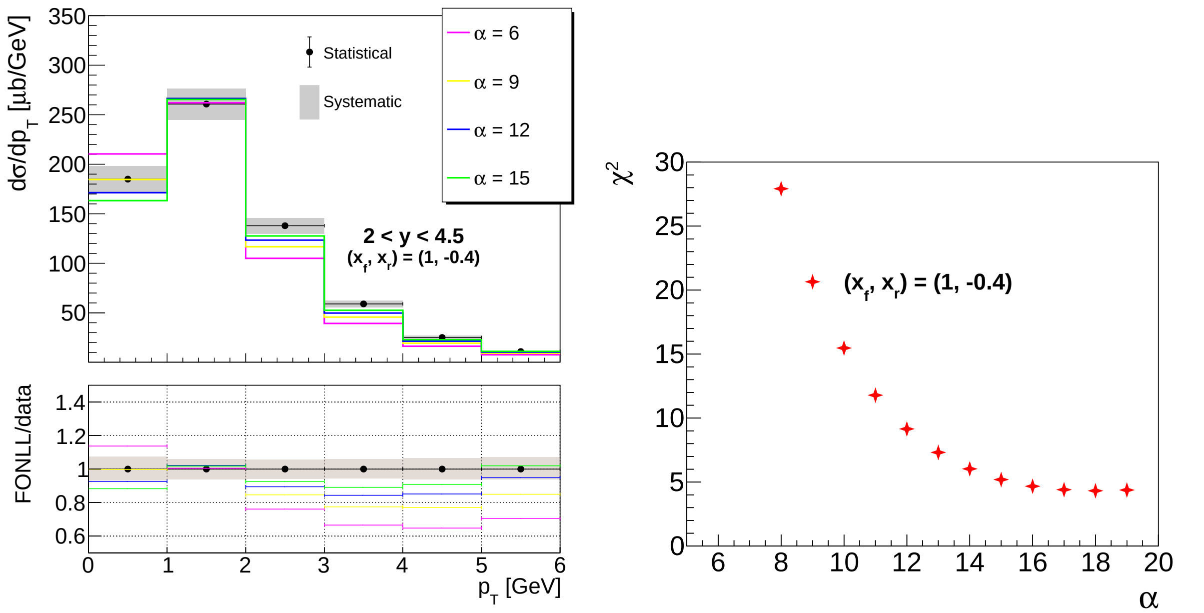

Figure 28: FONLL predictions with p_T-dependent c-hadron fractions and χ^2-test values with $f = 5$ d.o.f. for $\frac{d\sigma}{dp_T}$ together with LHCb data for different values of α.

2.3.4 Combined χ^2-test values for all three experiments

By summing up the χ^2 values obtained from ALICE, CMS and LHCb for all five scale sets, we are able to determine the best Kartvelishvili fragmentation parameter α (see Table 3). In the following, the combined χ^2 curves for every scale set are provided for reference as well.

$\chi^2(f = 21)$	Best Kartvelishvili parameter α	Scale Set (x_f, x_r)
14.0897	12	$(0, -0.95)$
11.5833	13	$(0.25, -0.8)$
12.3377	14	$(0.5, -0.65)$
14.6992	15	$(0.75, -0.5)$
14.9889	15	$(1.0, -0.4)$

Table 3: Result of the χ^2-test with $f = 21$ d.o.f. on p_T bins using y-integrated differential cross sections from ALICE, CMS and LHCb (see Table 1).

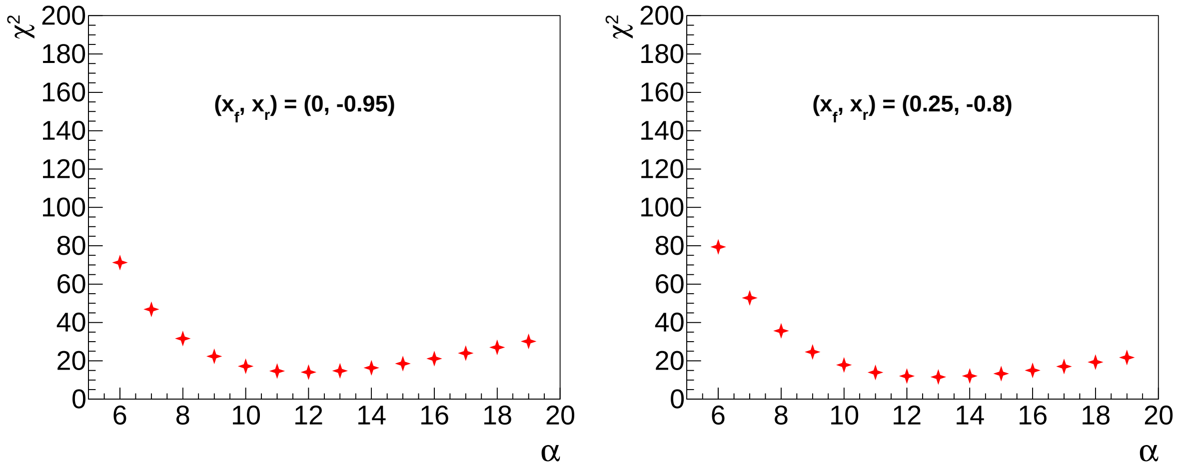

Figure 29: Combined χ^2 curve with $f = 21$ d.o.f. for comparing FONLL predictions to ALICE, CMS and LHCb data for 5 TeV D^0 meson production using a p_T-dependent c-hadron fraction.

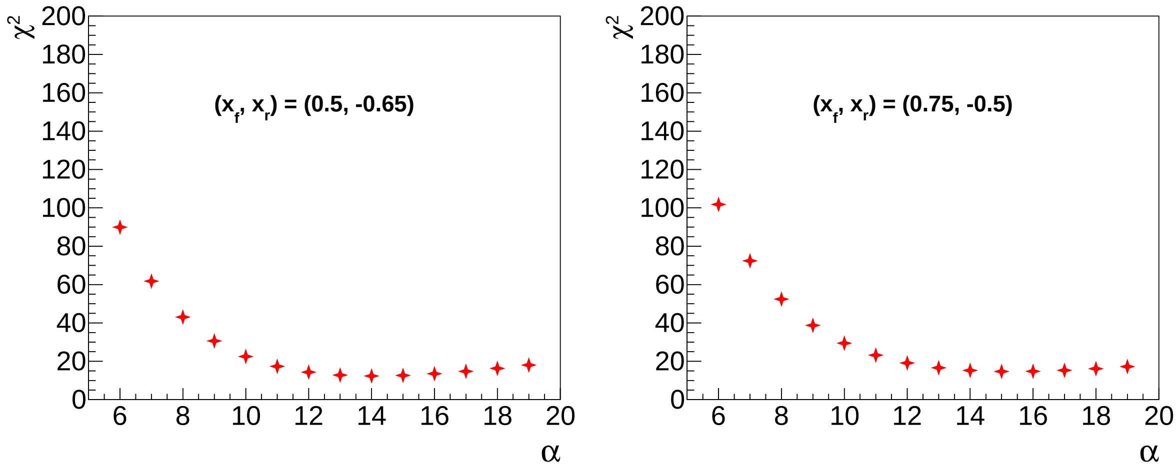

Figure 30: Combined χ^2 curve with $f = 21$ d.o.f. for comparing FONLL predictions to ALICE, CMS and LHCb data for 5 TeV D^0 meson production using a p_T-dependent c-hadron fraction.

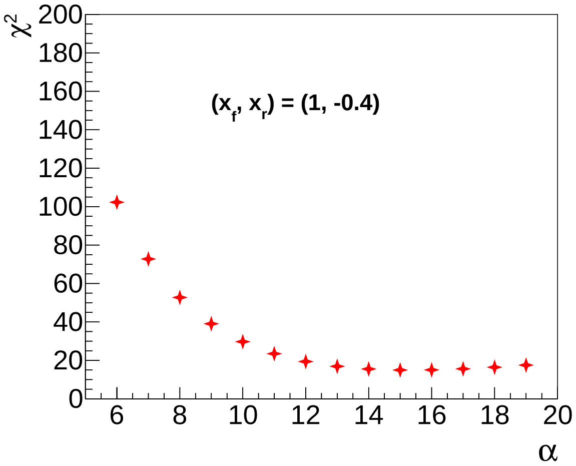

Figure 31: Combined χ^2 curve with $f = 21$ d.o.f. for comparing FONLL predictions to ALICE, CMS and LHCb data for 5 TeV D^0 meson production using a p_T-dependent c-hadron fraction.

2.4 Total c-quark and D^0 meson production cross section

In summary, our best choice of the scales (x_f, x_r) and the fragmentation parameter α allows us to extrapolate the c-quark production cross section to the full phase space $0 < p_T < 300$ GeV and $0 < y < 8.5$. Since we did not yet derive uncertainties for the three free parameters, we are only able to provide central values for each of the five scales.
Table 4 shows the FONLL prediction for the total c-quark production cross section and the total D^0 meson cross section (by applying the c-hadron fraction $f(c \to D^0) = 0.391$[2] to $\sigma_{c\bar{c}}$) using the best parameters. To actually extrapolate our D^0 meson cross section data, one would have to use ALICE, CMS or LHCb data, whenever they are available and cover the remaining phase space with FONLL predictions.

Central value	$\sigma_{c\bar{c}}$ [mb]	$\sigma_{\frac{D^0+\overline{D^0}}{2}}$ [mb]	$\chi^2_{\mathrm{central}}(f=21)$	$\alpha(\chi^2(f=21))$
$\mu_f = \mu_0,\ \mu_r = 2^{-0.95}\mu_0$	4.126	1.613	7.34512	12(14.0897)
$\mu_f = 2^{+0.25}\mu,\ \mu_r = 2^{-0.8}\mu_0$	4.198	1.641	6.46289	13(11.5833)
$\mu_f = 2^{+0.5}\mu,\ \mu_r = 2^{-0.65}\mu_0$	4.181	1.634	5.71467	14(12.3377)
$\mu_f = 2^{+0.75}\mu,\ \mu_r = 2^{-0.5}\mu_0$	4.124	1.612	5.41831	15(14.6992)
$\mu_f = 2\mu_0,\ \mu_r = 2^{-0.4}\mu_0$	4.151	1.623	5.40474	15(14.9889)

Table 4: FONLL prediction, assuming p_T-dependent c-hadron fractions, for the total c-quark and D^0 meson production cross section ($0 < p_T < 300$ GeV and $0 < y < 8.5$) together with best FONLL input parameters, derived from 5 TeV D^0 meson production together with the best free parameters and corresponding χ^2 values.

3 Extrapolation of D^* meson cross section measured at 7 TeV in LHC

Experiment	y range	p_T range	Reference
CMS	$\lvert y\rvert < 2.5$	$p_T > 1$ GeV	not yet published
LHCb	$2.0 < y < 2.5$	$3 < p_T < 8$ GeV	[12]
	$2.5 < y < 3.0$	$1 < p_T < 8$ GeV	
	$3.0 < y < 3.5$	$0 < p_T < 7$ GeV	
	$3.5 < y < 4.0$	$0 < p_T < 7$ GeV	
	$4.0 < y < 4.5$	$0 < p_T < 5$ GeV	

Table 5: Used measurements for differential production cross sections of D^* mesons at $\sqrt{s} = 7$ TeV pp-collision and their kinematic ranges for the rapidity y and transverse momentum p_T.

Thanks to our preliminary 5 TeV study, we were able to determine initial parameters for the two scales $(x_f, x_r) = (0, -0.95)$ and the fragmentation parameter $\alpha = 11$. Since our scale set from the 5 TeV study is very close to the theoretically motivated scale set $(x_f, x_r) = (0, -1.0)$ from b-quark production at HERA (see [13], chapter 2.11), we vary the scales around $(x_f, x_r) = (0, -1.0)$ instead. As before, an overview of the used measurements from CMS and LHCb can be found in Table 5.

Since the transverse momentum p_T does not cover the whole kinematic region $0 < p_T < 8$ GeV for all rapidity bins, we are unable to study p_T or y integrated differential cross sections and thus treat y and p_T as independent, as we did in the 5 TeV study before.

This lack of coverage of our data forces us to always look at the double-differential cross section $\frac{\mathrm{d}^2\sigma}{\mathrm{d}p_T\mathrm{d}y}$. To still retain two-dimensional plots, we choose to create p_T-distribution plots for every rapidity bin, in which we vary the scales (x_f, x_r) and the fragmentation parameter around our initial parameters.

3.1 Determining initial α of the Kartvelishvili fragmentation function from FONLL

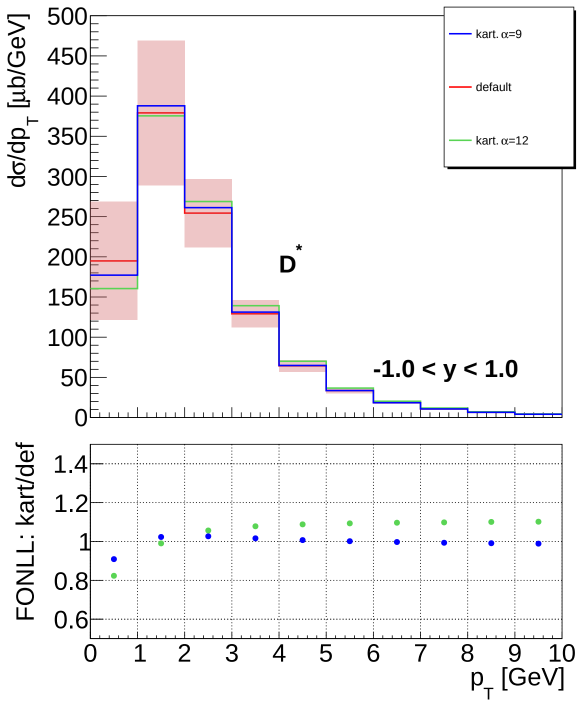

Figure 32: FONLL predictions for y-integrated $(-1.0 < y < 1.0)$ p_T-differential D^* meson cross section using the default fragmentation from the web tool (http://www.lpthe.jussieu.fr/ cacciari/fonll/fonll-form.html) and Kartvelishvili fragmentation using $\alpha = 9$ and $\alpha = 12$.

In addition to including $\alpha = 11$ in our variation, we choose to determine the initial value for α from a comparison of the y-integrated $(-1.0 < y < 1.0)$ p_T-differential D^* meson cross section using the default fragmentation from the web tool (http://www.lpthe.jussieu.fr/ cacciari/fonll/fonllform.html) and Kartvelishvili fragmentation using $\alpha = 9$ and $\alpha = 12$ (see Figure 32). We naïvely assume the web tool's FONLL predictions to most closely resemble actual D^* cross section data and thus choose $\alpha = 9$ as the central value for the Kartvelishvili fragmentation.

In summary, we choose to vary $\alpha \pm 6$ around $\alpha = 9$; regarding the scales, we choose to vary $x_r \pm 0.25$ and $x_f + 2 \cdot 0.25 - 0.2$ [2] around $(x_f, x_r) = (0, -1.0)$ since the slope of the interpolation line in Figure 12 has shown that our studied scale sets are less sensitive to variations in x_f than in x_r. In the following p_T-distribution plots, the last bin (displayed as $10\,\text{GeV} < p_T < \infty$) denotes the p_T-overflow bin, covering all of the remaining phase space with respect to p_T.

To provide another view on the double-differential cross sections and better visualize the interplay of CMS and LHCb data, we also created y-distribution plots, which can be found in the appendix (see subsection 5.2).

[2] We cannot go down to $x_f = -0.25$ since our PDF set would not provide consistent results on such low values of μ_f. For a detailed discussion, please see [7], slide 22

3.2 Variation of x_f

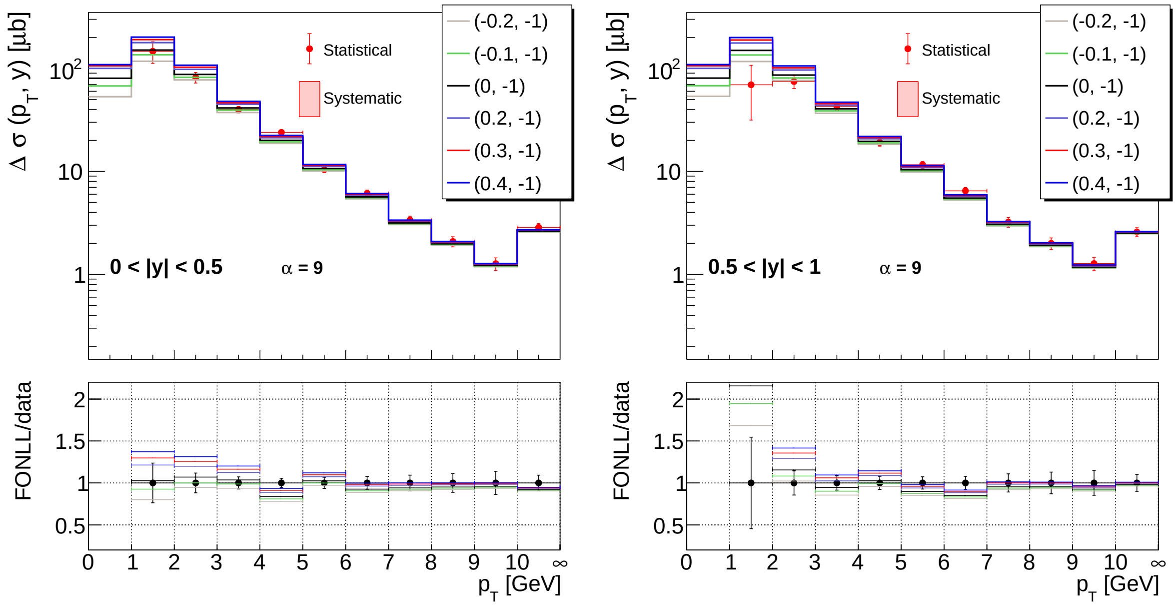

Figure 33: FONLL predictions with p_T-dependent c-hadron fractions for $\Delta\sigma(p_T, y)$ together with CMS data for different values of x_f while keeping $x_r = -1$ and $\alpha = 9$ fixed (two-tuple notation: (x_f, x_r)).

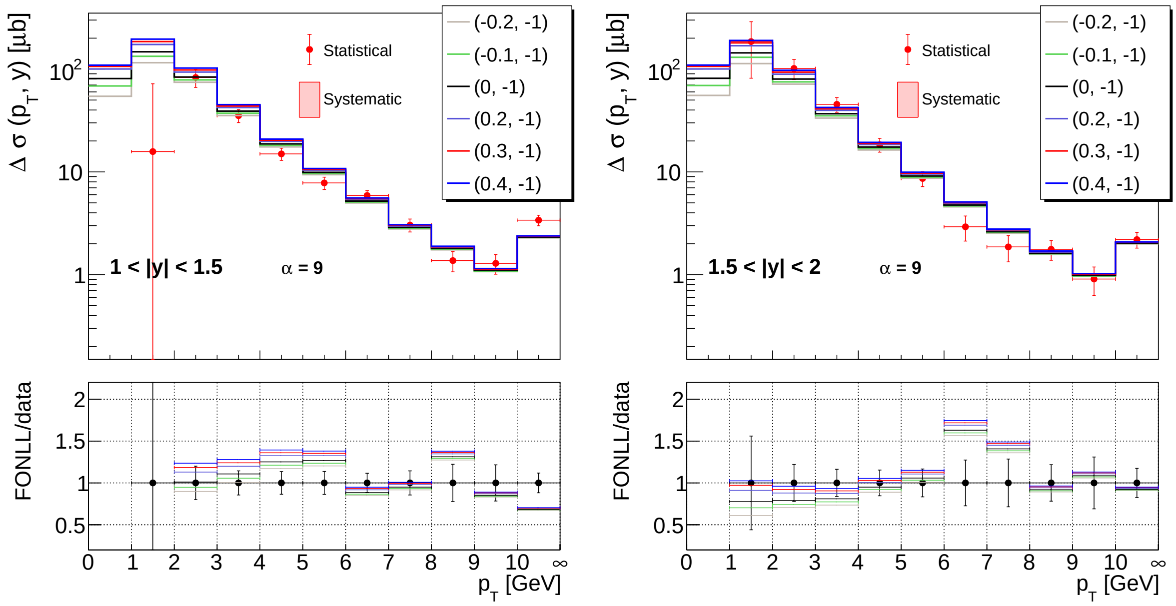

Figure 34: FONLL predictions with p_T-dependent c-hadron fractions for $\Delta\sigma(p_T, y)$ together with CMS data for different values of x_f while keeping $x_r = -1$ and $\alpha = 9$ fixed (two-tuple notation: (x_f, x_r)).

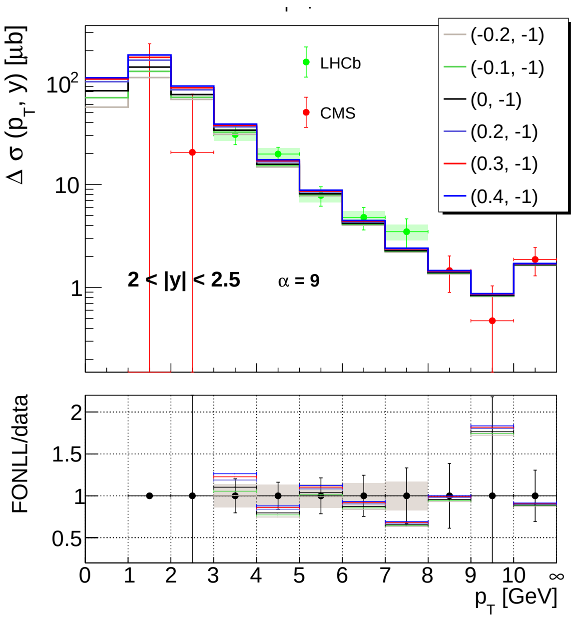

Figure 35: FONLL predictions with p_T-dependent c-hadron fractions for $\Delta\sigma(p_T, y)$ together with CMS and LHCb data for different values of x_f while keeping $x_r = -1$ and $\alpha = 9$ fixed (two-tuple notation: (x_f, x_r)).

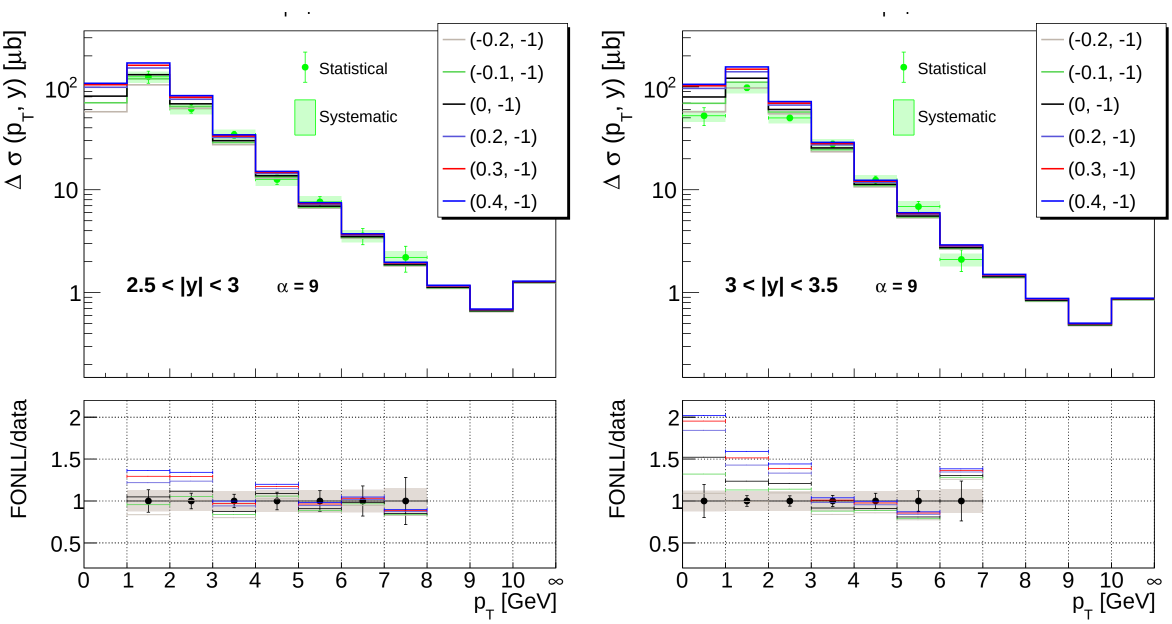

Figure 36: FONLL predictions with p_T-dependent c-hadron fractions for $\Delta\sigma(p_T, y)$ together with LHCb data for different values of x_f while keeping $x_r = -1$ and $\alpha = 9$ fixed (two-tuple notation: (x_f, x_r)).

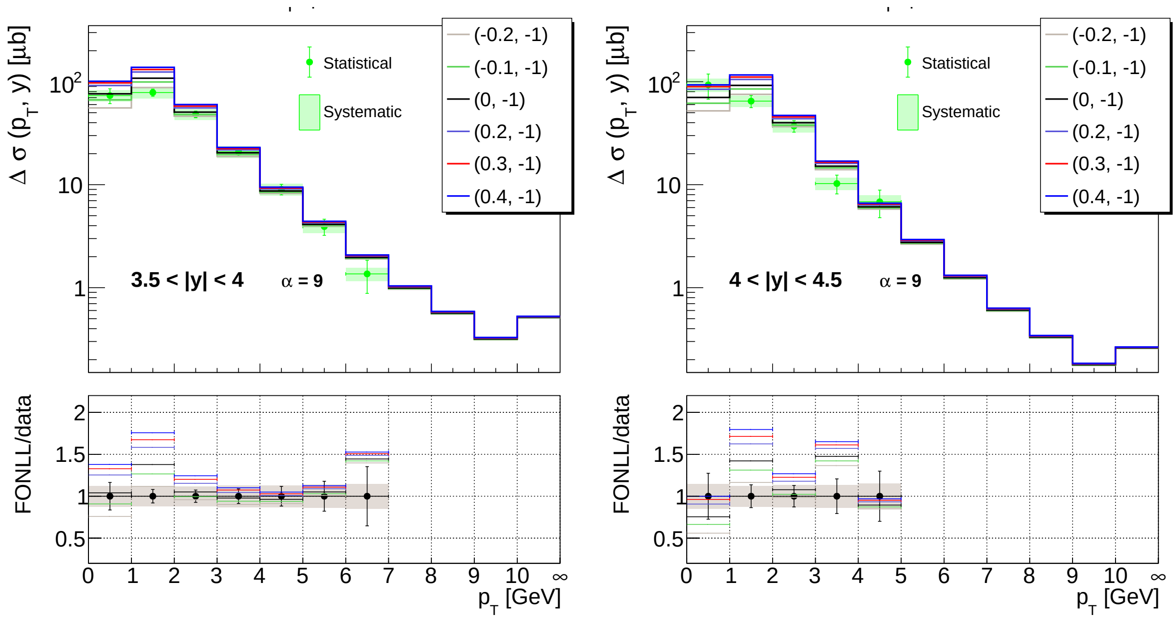

Figure 37: FONLL predictions with p_T-dependent c-hadron fractions for $\Delta\sigma(p_T, y)$ together with LHCb data for different values of x_f while keeping $x_r = -1$ and $\alpha = 9$ fixed (two-tuple notation: (x_f, x_r)).

3.3 Variation of x_r

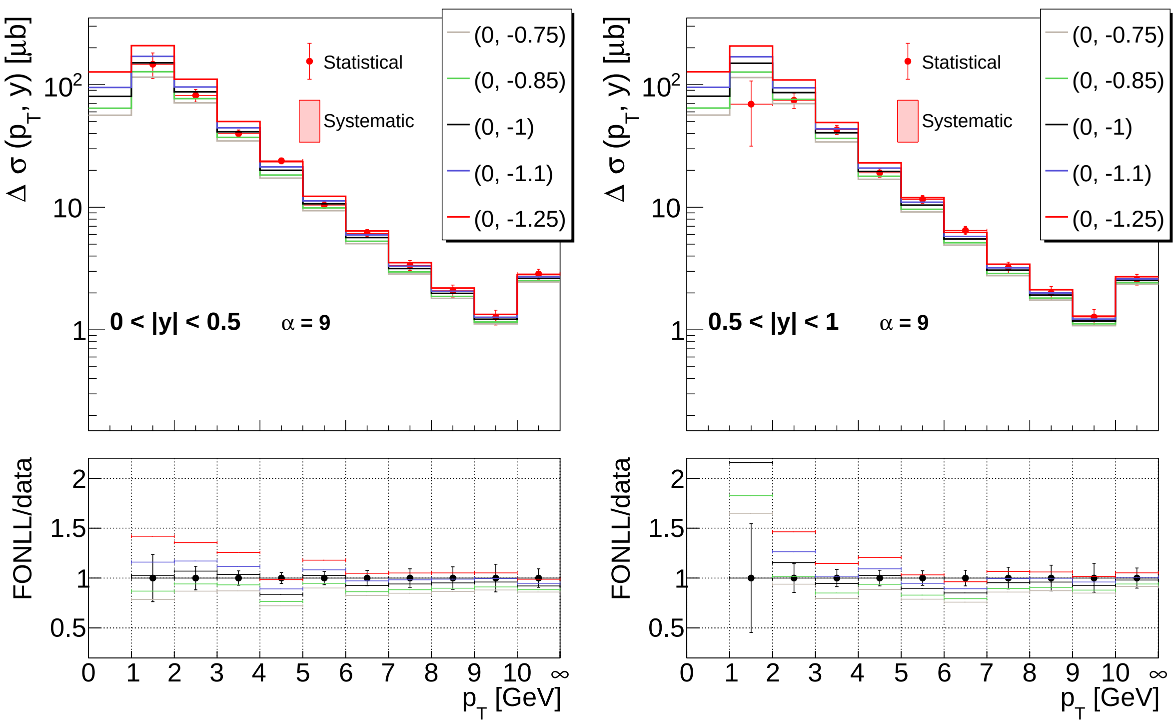

Figure 38: FONLL predictions with p_T-dependent c-hadron fractions for $\Delta\sigma(p_T, y)$ together with CMS data for different values of x_r while keeping $x_f = 0$ and $\alpha = 9$ fixed (two-tuple notation: (x_f, x_r)).

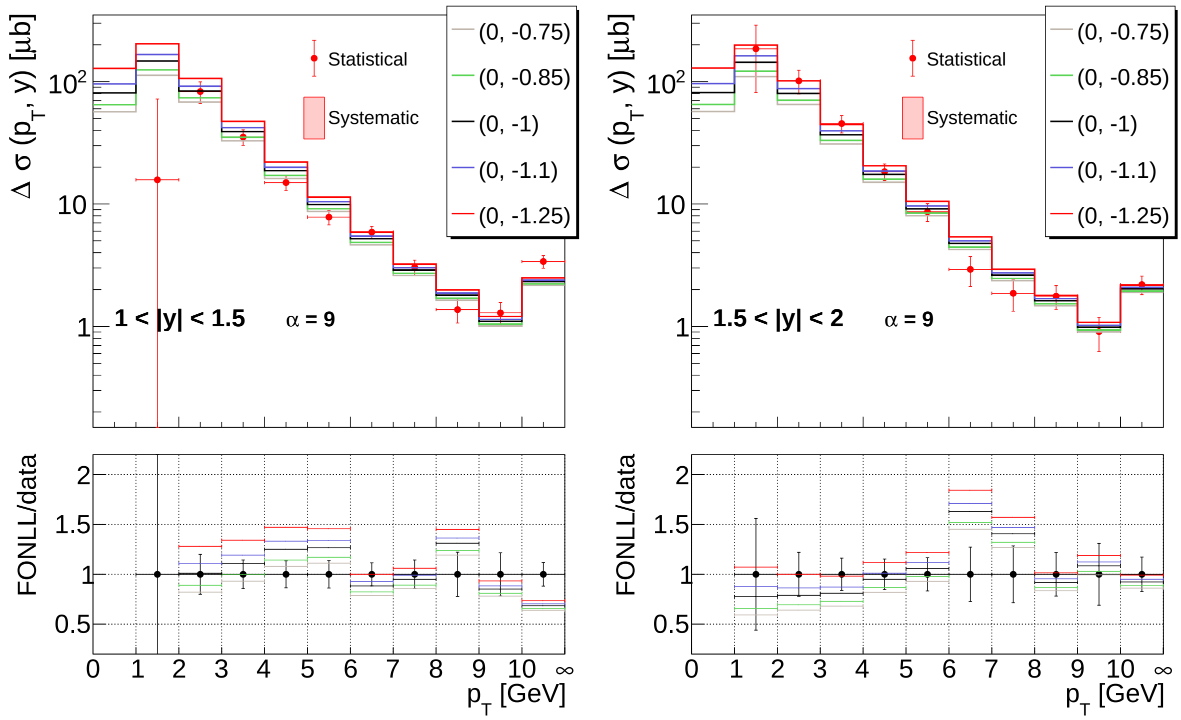

Figure 39: FONLL predictions with p_T-dependent c-hadron fractions for $\Delta\sigma(p_T, y)$ together with CMS data for different values of x_r while keeping $x_f = 0$ and $\alpha = 9$ fixed (two-tuple notation: (x_f, x_r)).

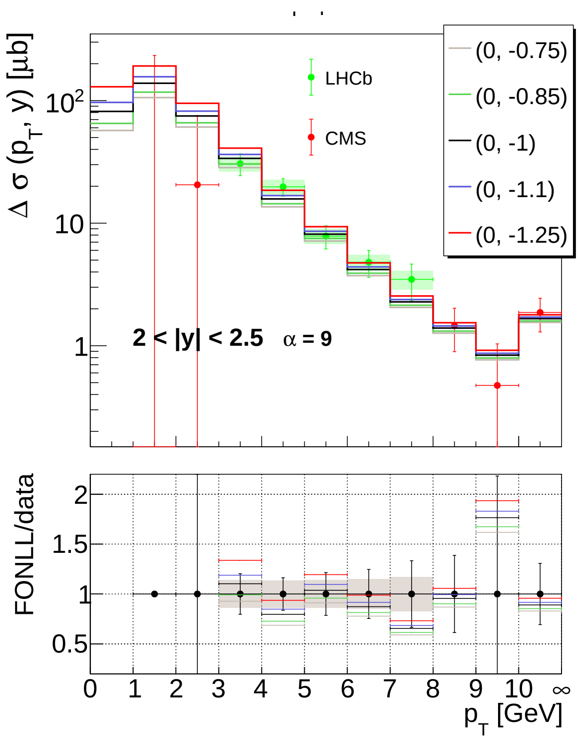

Figure 40: FONLL predictions with p_T-dependent c-hadron fractions for $\Delta\sigma(p_T, y)$ together with CMS and LHCb data for different values of x_r while keeping $x_f = 0$ and $\alpha = 9$ fixed (two-tuple notation: (x_f, x_r)).

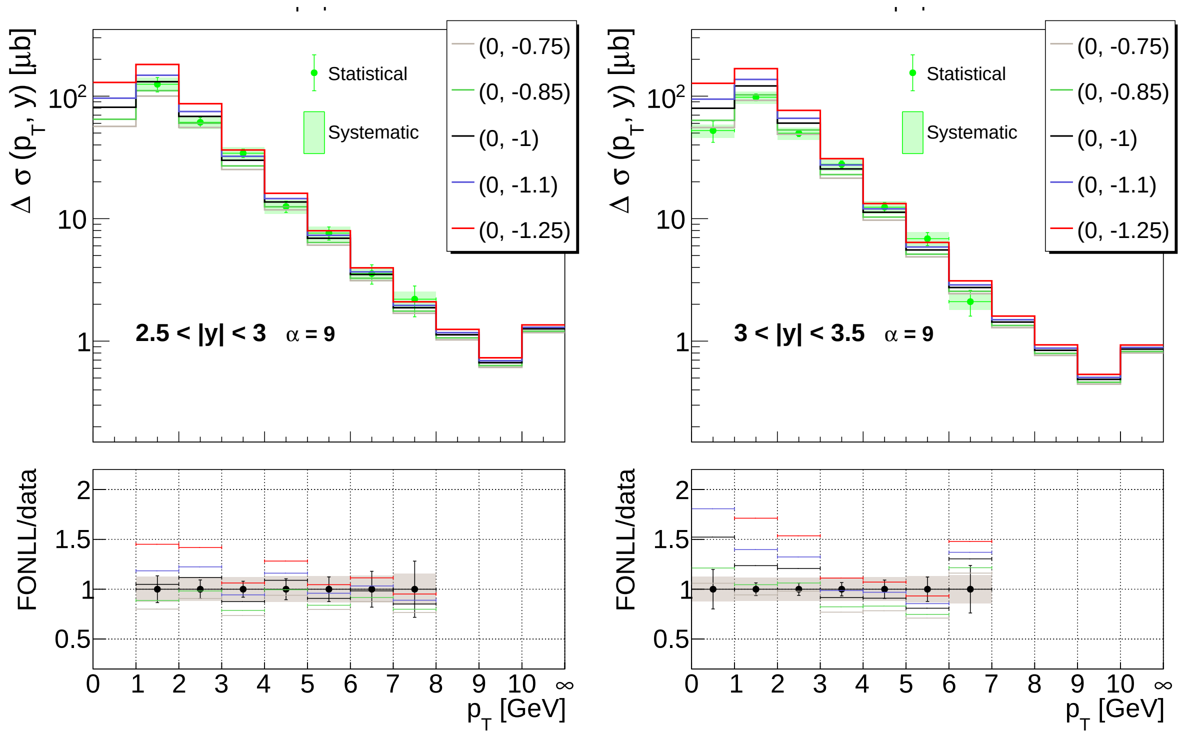

Figure 41: FONLL predictions with p_T-dependent c-hadron fractions for $\Delta\sigma(p_T, y)$ together with LHCb data for different values of x_r while keeping $x_f = 0$ and $\alpha = 9$ fixed (two-tuple notation: (x_f, x_r)).

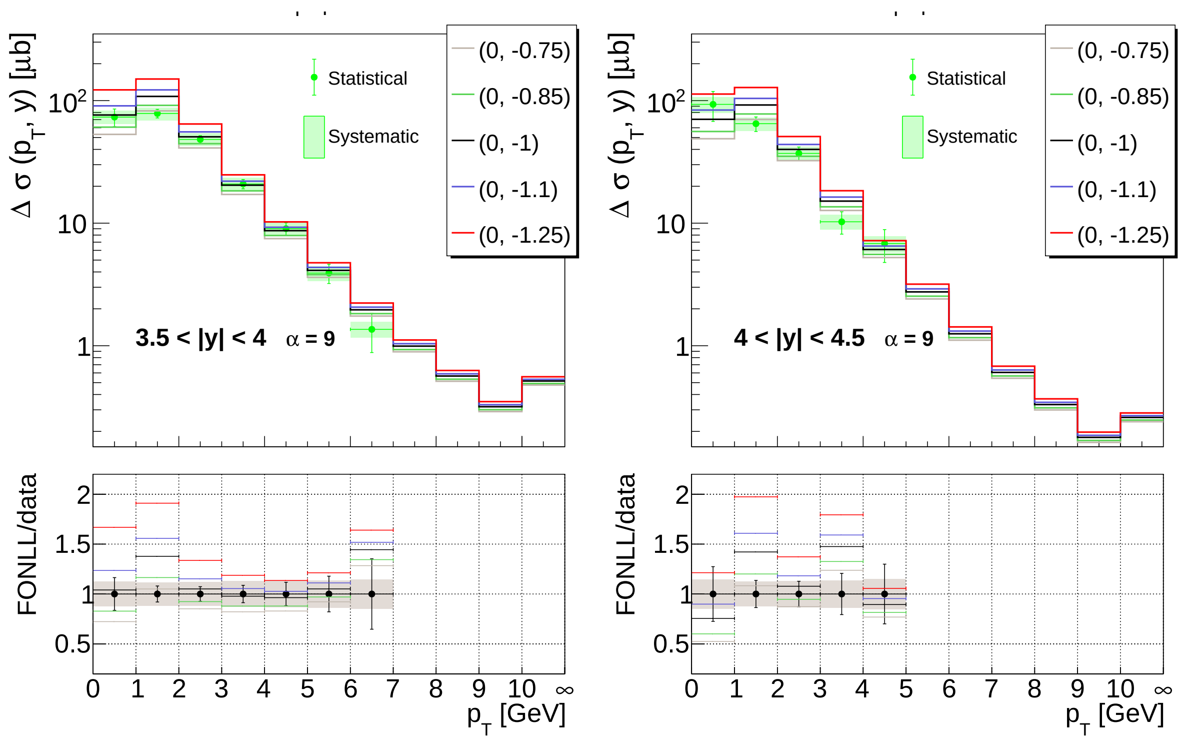

Figure 42: FONLL predictions with p_T-dependent c-hadron fractions for $\Delta\sigma(p_T, y)$ together with LHCb data for different values of x_r while keeping $x_f = 0$ and $\alpha = 9$ fixed (two-tuple notation: (x_f, x_r)).

3.4 Variation of α

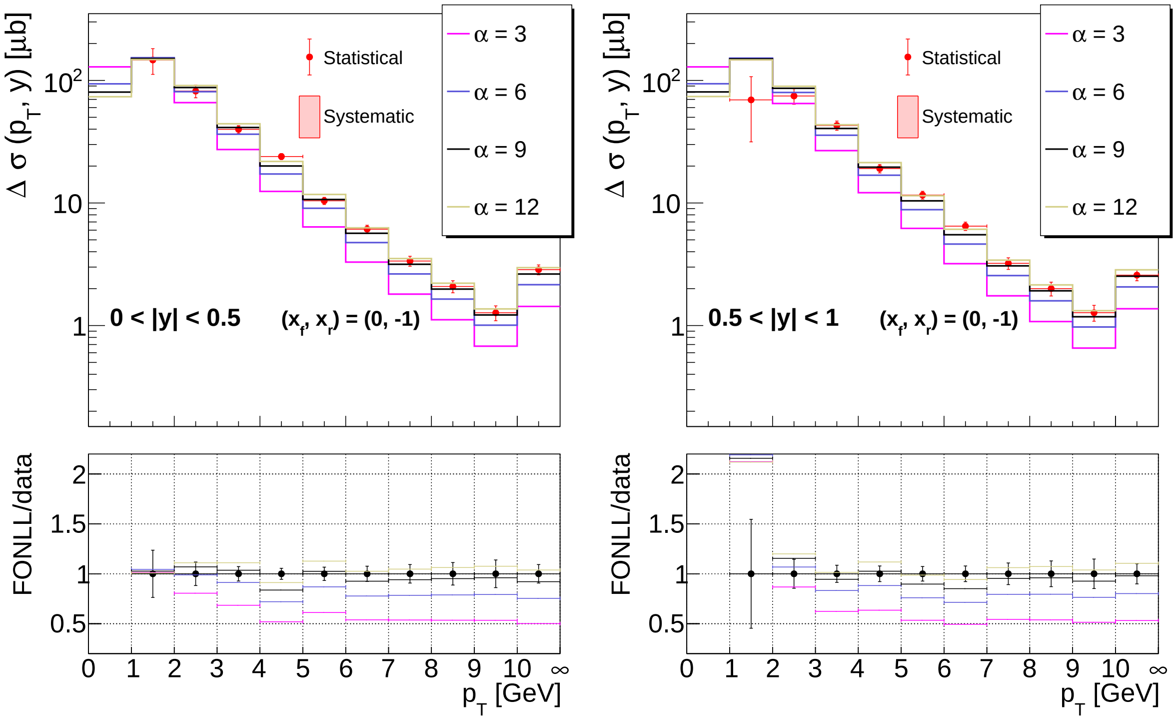

Figure 43: FONLL predictions with p_T-dependent c-hadron fractions for $\Delta\sigma(p_T, y)$ together with CMS data for different values of α while keeping $x_f = 0$ and $x_r = -1$ fixed.

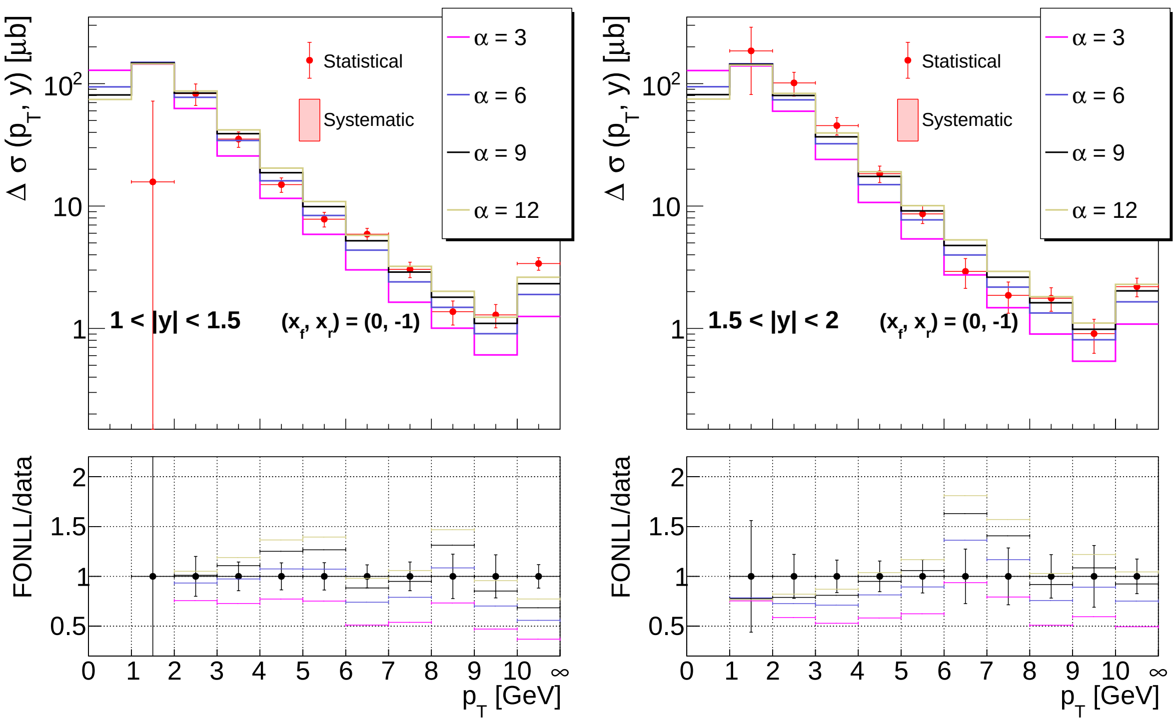

Figure 44: FONLL predictions with p_T-dependent c-hadron fractions for $\Delta\sigma(p_T, y)$ together with CMS data for different values of α while keeping $x_f = 0$ and $x_r = -1$ fixed.

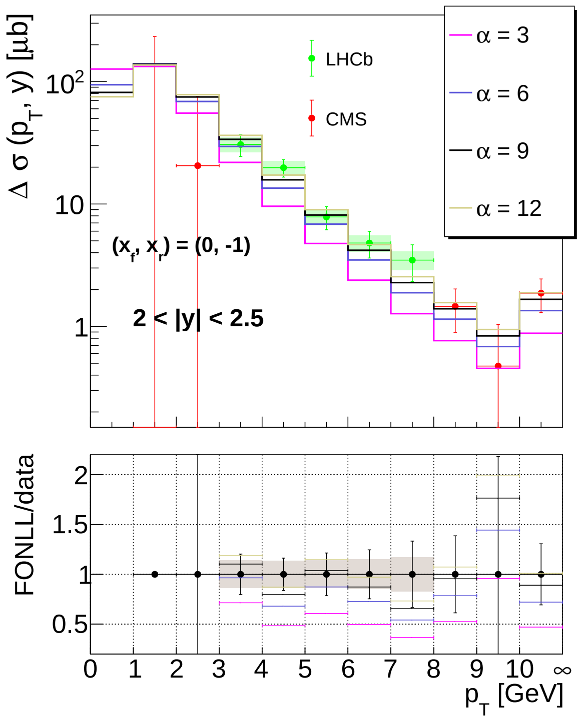

Figure 45: FONLL predictions with p_T-dependent c-hadron fractions for $\Delta\sigma(p_T, y)$ together with CMS and LHCb data for different values of α while keeping $x_f = 0$ and $x_r = -1$ fixed.

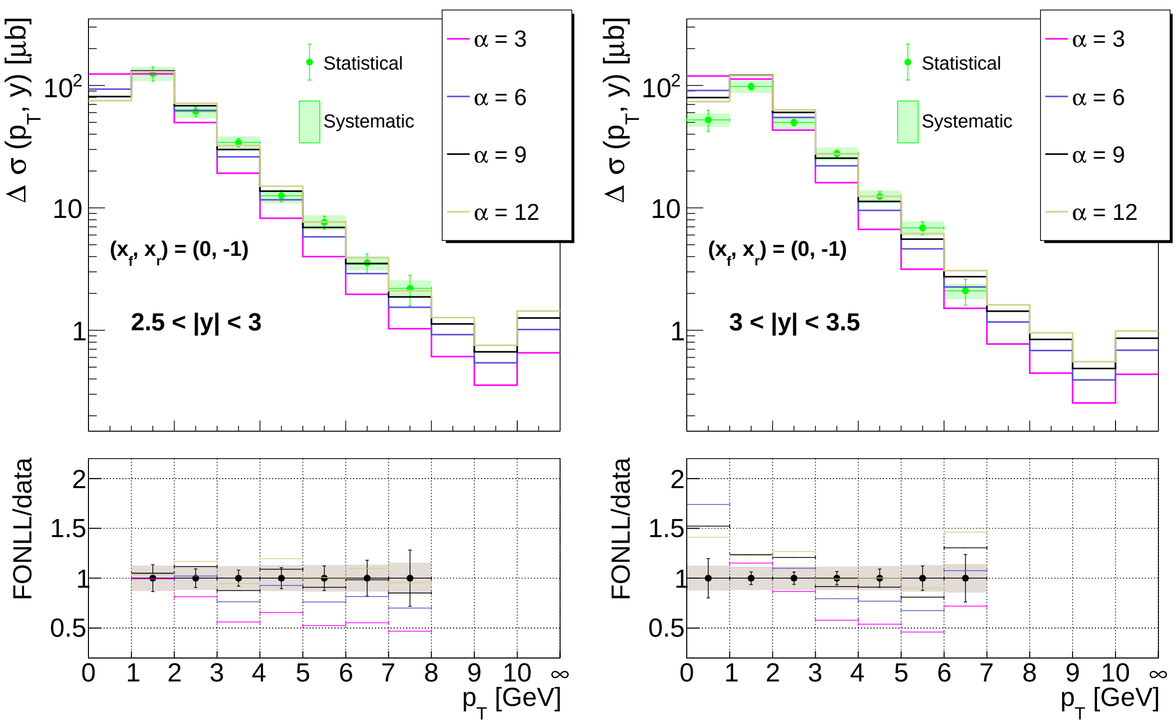

Figure 46: FONLL predictions with p_T-dependent c-hadron fractions for $\Delta\sigma(p_T, y)$ together with LHCb data for different values of α while keeping $x_f = 0$ and $x_r = -1$ fixed.

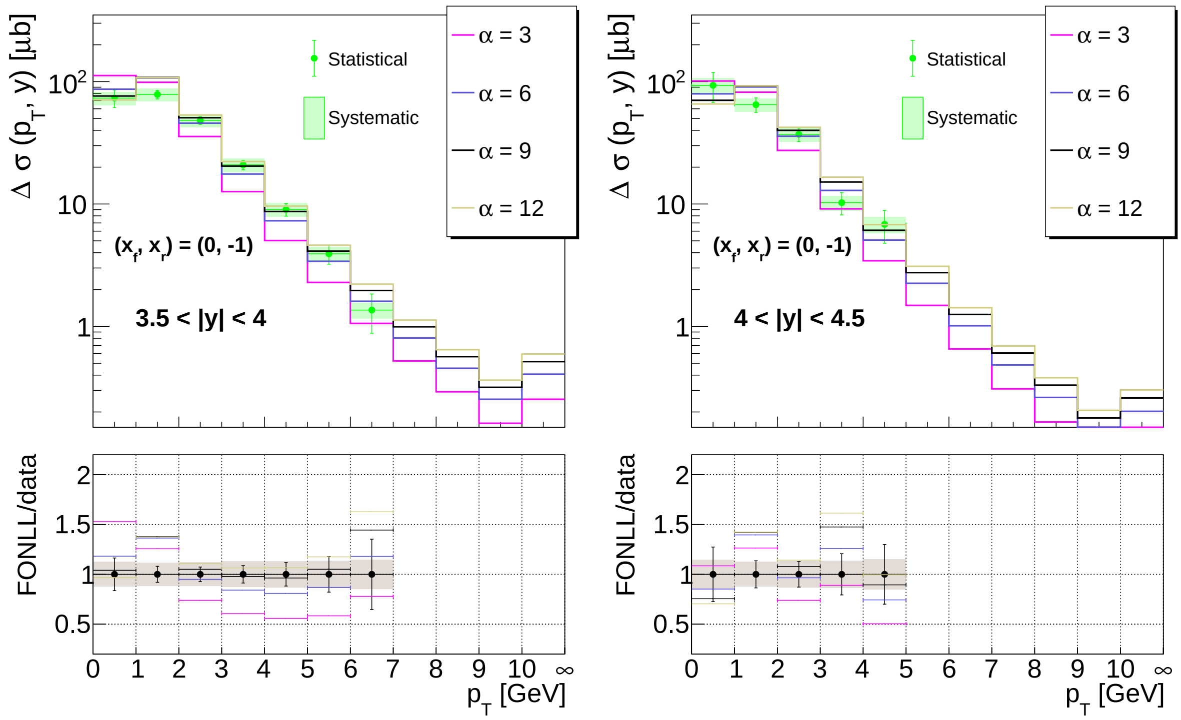

Figure 47: FONLL predictions with p_T-dependent c-hadron fractions for $\Delta\sigma(p_T, y)$ together with LHCb data for different values of α while keeping $x_f = 0$ and $x_r = -1$ fixed.

3.4.1 Combined χ^2 curves for CMS and LHCb

By summing up the χ^2 values obtained from CMS and LHCb for varying x_f, x_r and α around our initial values $((x_f, x_r) = (0, -1)$ and $\alpha = 9)$ independently, we are able to determine the best parameters (see Table 6). In the following, the combined χ^2 curves for every variation are provided for reference as well.

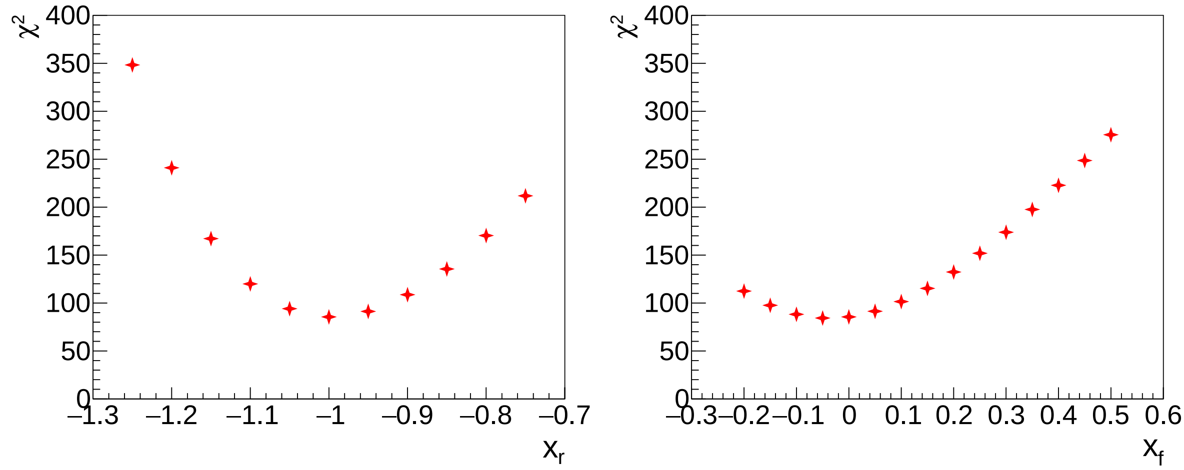

Figure 48: Combined χ^2 curve for comparing FONLL predictions to CMS and LHCb data for 7 TeV D^* meson production using a p_T-dependent c-hadron fraction. For the variation of x_r the scale $x_f = 0.0$ has been fixed (left plot); for x_f respectively $x_r = -1.0$ (right plot).

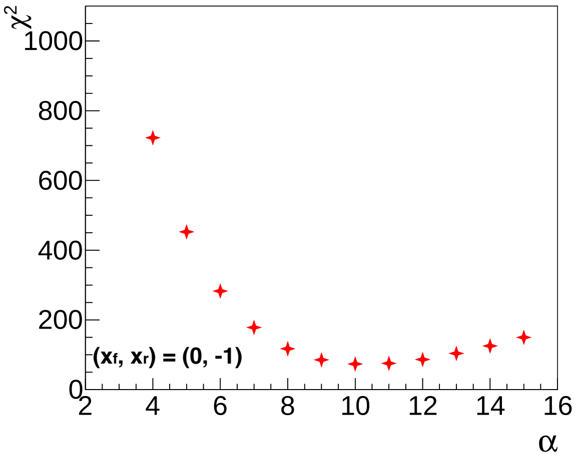

Figure 49: Combined χ^2 curve for comparing FONLL predictions to CMS and LHCb data for 7 TeV D^* meson production using a p_T-dependent c-hadron fraction. The varied quantity is the Kartvelishvili fragmentation parameter α, while the scale set has been fixed to $(x_f, x_r) = (0.0, -1.0)$.

χ^2	Best parameter
84.3272	$x_f = -0.05$
85.5069	$x_r = -1.0$
73.6454	$\alpha = 10$

Table 6: Best parameters by $\chi^2(f = 75)$ on double differential cross sections of 7 TeV D^* meson production from CMS and LHCb (see Table 1).

3.5 Total c-quark and D^* meson production cross section

Analogously to subsection 2.4, we can extrapolate the c-quark production and D^* meson cross section to the full phase space $0 < p_T < 300$ GeV and $0 < y < 8.5$. Since we did not yet derive uncertainties for the three free parameters, we are only able to provide central values for the two scales (x_f, x_r) and the fragmentation parameter α and thus the cross section.
Table 4 shows the FONLL prediction for the total c-quark production cross section and the total D^* meson cross section (by applying the c-hadron fraction $f(c \to D^{*,+}) = 0.155$[2] to $\sigma_{c\bar{c}}$) using the best parameters. To actually extrapolate our D^* meson cross section data, one would have to use CMS or LHCb data, whenever they are available and cover the remaining phase space with FONLL predictions.

Central value	$\sigma_{c\bar{c}}$ [mb]	$\sigma_{\frac{D^{*,+}+D^{*,-}}{2}}$ [mb]	$\chi^2_{x_f}(f = 75)$	$\chi^2_{x_r}(f = 75)$	$\alpha(\chi^2(f = 75))$
$\mu_f = 2^{-0.05}\mu_0,\ \mu_r = 2^{-1.0}\mu$	5.347	0.828	84.3272	85.5069	10(73.6454)

Table 7: FONLL prediction, assuming p_T-dependent c-hadron fractions, for the total c-quark and D^* meson production cross section ($0 < p_T < 300$ GeV and $0 < y < 8.5$) together with best FONLL input parameters, derived from 7 TeV D^* meson cross section together with the best free parameters and corresponding χ^2 values.

4 Conclusion

In conclusion, this summer student project both updated last year's preliminary study with 5 TeV D^0 meson measurements [7] with up-to-date empirical data, suggesting a collision-system and p_T-dependence of c-hadron fragmentation fractions (see section 2) and also made first steps toward an extrapolation (or respectively interpolation) of not yet published D^* meson cross sections, measured in the CMS experiment in LHC at 7 TeV (see section 3).

With regards to the 5 TeV D^0 study, an interesting comparison of the shape of FONLL p_T-distribution data assuming p_T-(in)dependent c-hadron fractions is made possible (see subsection 2.3 and subsection 5.1): while applying a p_T-independent c-hadron fraction requires a Kartvelishvili fragmentation parameter $15 < \alpha < 24$, which has to go up to $\alpha = 23$ for the scale set $(x_f, x_r) = (1.0, -0.4)$, p_T-dependent fractions make FONLL predictions describe the experimental data well already with $\alpha < 16$ for all five scale sets.
Nonetheless it is noteworthy that the $\chi^2(f = 21)$ values for p_T-independent fractions are consistently $\mathcal{O}(1)$ to $\mathcal{O}(3)$ lower than their p_T-dependent counterparts (see Table 3 and Table 8), hinting at an overall better description of the data. This however does not seem plausible when looking at Figure 14: While a Kartvelishvili fragmentation parameter of $\alpha = 11$ describes the data best by χ^2, the FONLL prediction with $\alpha = 6$ fits the shape of the ALICE data much better. It is only because of the concrete normalization imposed by the choice of the scale set $(x_f, x_r) = (0.0, -1.0)$ that $\alpha = 11$ has a lower χ^2 value than $\alpha = 6$.
Thus - in a future work - one could treat the normalization as an additional free parameter or choose a better adjusted scale set to find the best value of α.

Concerning the 7 TeV D^* meson study, we were able to find suitable FONLL parameters (see Table 6) by varying around initial values $(x_f, x_r) = (0.0, -1.0)$ and $\alpha = 9$, motivated by a theoretical argument in [13], our 5 TeV D^0 meson study and a comparison of Kartvelishvili fragmentation with the default fragmentation from the FONLL web tool (see subsection 3.1). Although the currently unpublished CMS data does not yet include systematic uncertainties, we were able to obtain preliminary results, which - in the future - can be used to extrapolate the measured data and c-quark cross section to the full phase space. In addition to including systematic uncertainties one should then also derive uncertainties for the scale set (x_f, x_r) and the Kartvelishvili parameter α from variation of $\Delta\chi^2$ around the best values $(x_f, x_r) = (-0.05, -1.0)$ and $\alpha = 10$ (see Table 6).
In closing, our best Kartvelishvili fragmentation parameter $\alpha = 10$, compared with the results from [14] (see Table 4, extracted from LEP data), and also our best scale set $(x_f, x_r) = (-0.05, -1.0)$ are in good agreement with experimental data and theoretical expectations[14, 13].

Acknowledgements I would like to especially thank Achim and Yewon for the excellent supervision and the interesting topic. During my research, I always felt well integrated and enjoyed participating in current research. In conclusion, I am very grateful to have had the opportunity to do science at DESY!

5 Appendix

5.1 p_T-distributions for 5 TeV D^0 meson production with p_T-independent c-hadron fractions

Contrary to the FONLL predictions used in subsection 2.3, we did not apply a p_T-dependent correction to the c-hadron fraction for D^0 mesons (measured in ALICE, see [2]) here. This allows us to do a direct comparison between p_T-dependent and p_T-independent c-hadron fractions. Thus we repeated the steps of finding a suitable fragmentation parameter α here and can compare it to our p_T-dependent result in subsection 2.3.

ALICE

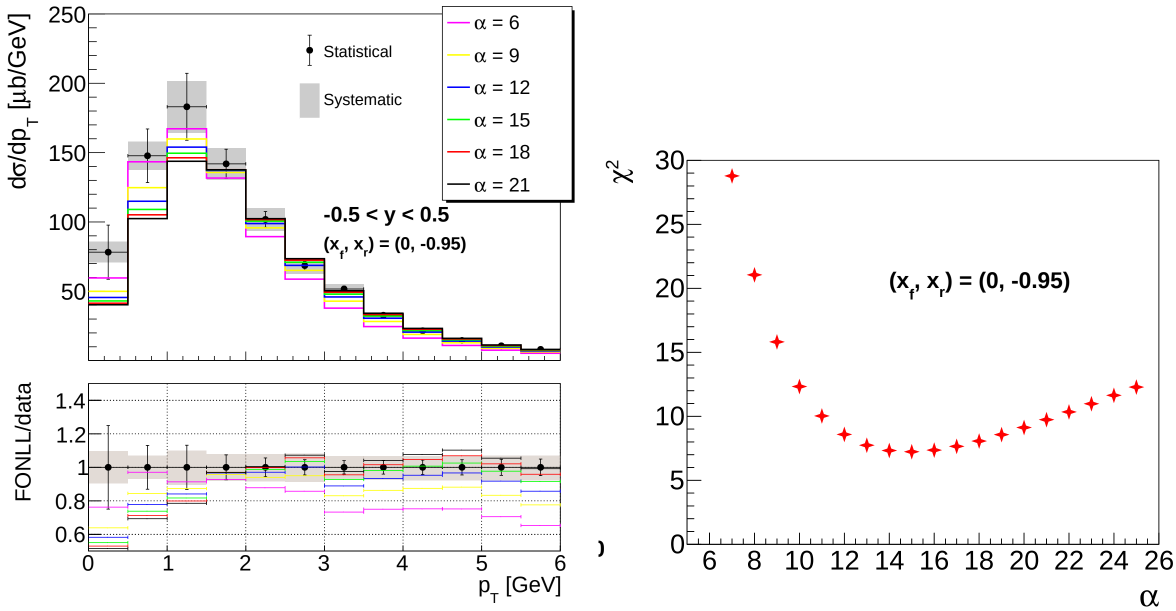

Figure 50: FONLL predictions with p_T-independent c-hadron fractions and χ^2-test values for $\frac{d\sigma}{dp_T}$ together with ALICE data for different values of α.

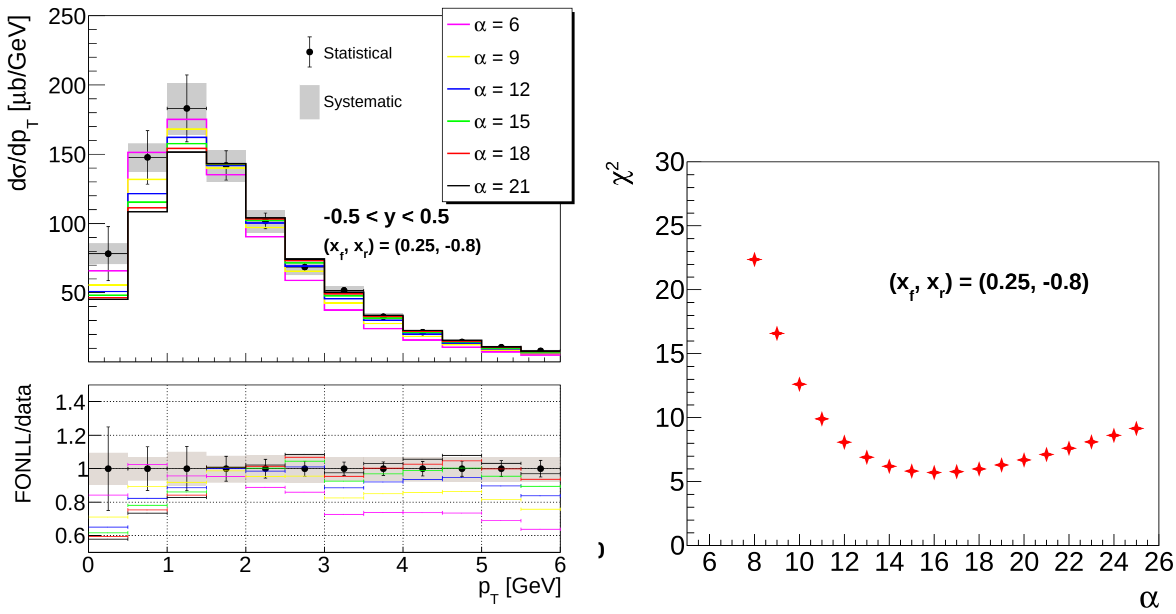

Figure 51: FONLL predictions with p_T-independent c-hadron fractions and χ^2-test values for $\frac{d\sigma}{dp_T}$ together with ALICE data for different values of α.

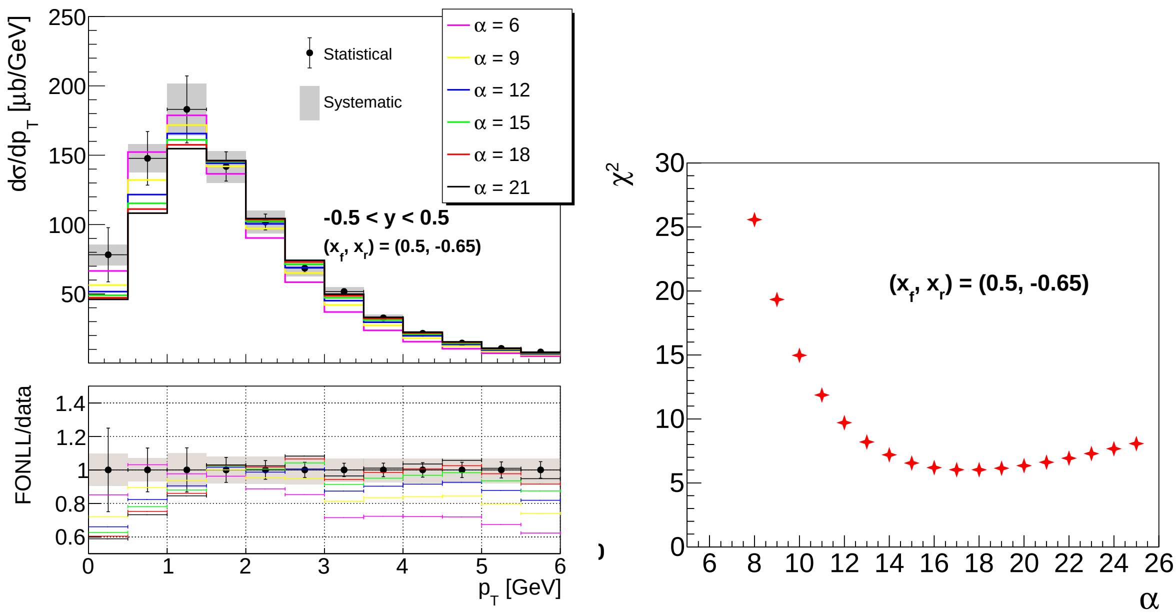

Figure 52: FONLL predictions with p_T-independent c-hadron fractions and χ^2-test values for $\frac{d\sigma}{dp_T}$ together with ALICE data for different values of α.

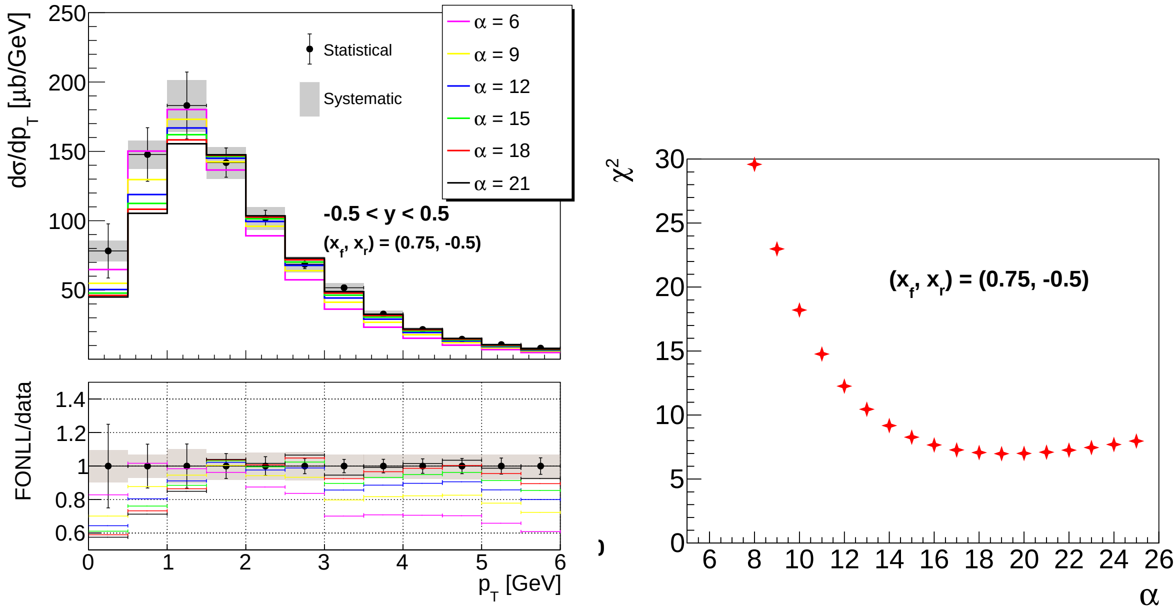

Figure 53: FONLL predictions with p_T-independent c-hadron fractions and χ^2-test values for $\frac{d\sigma}{dp_T}$ together with ALICE data for different values of α.

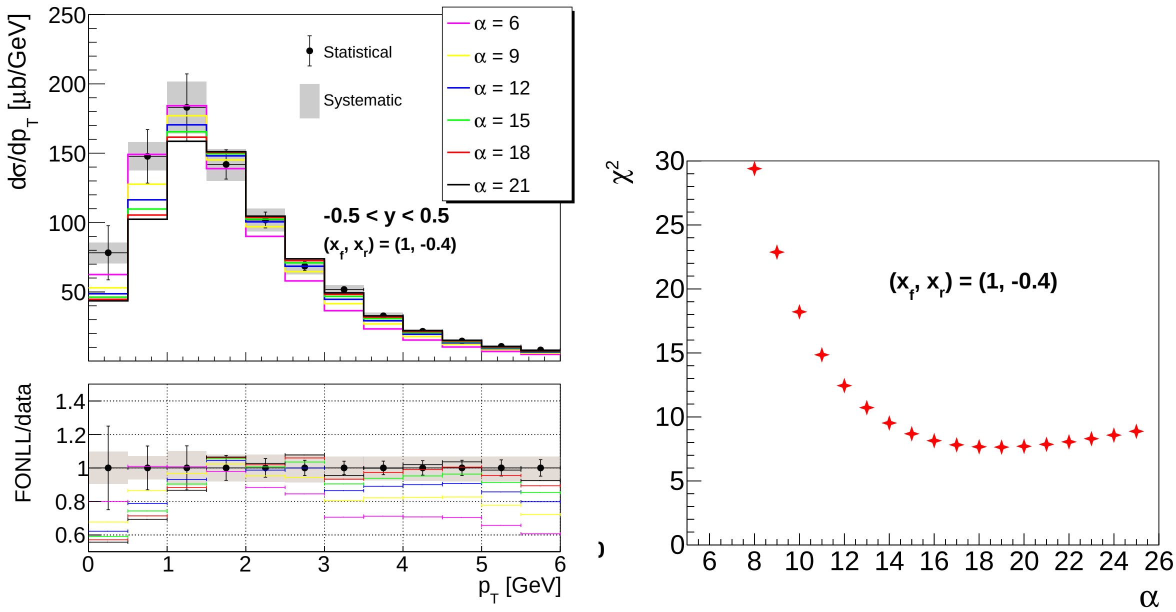

Figure 54: FONLL predictions with p_T-independent c-hadron fractions and χ^2-test values for $\frac{d\sigma}{dp_T}$ together with ALICE data for different values of α.

CMS

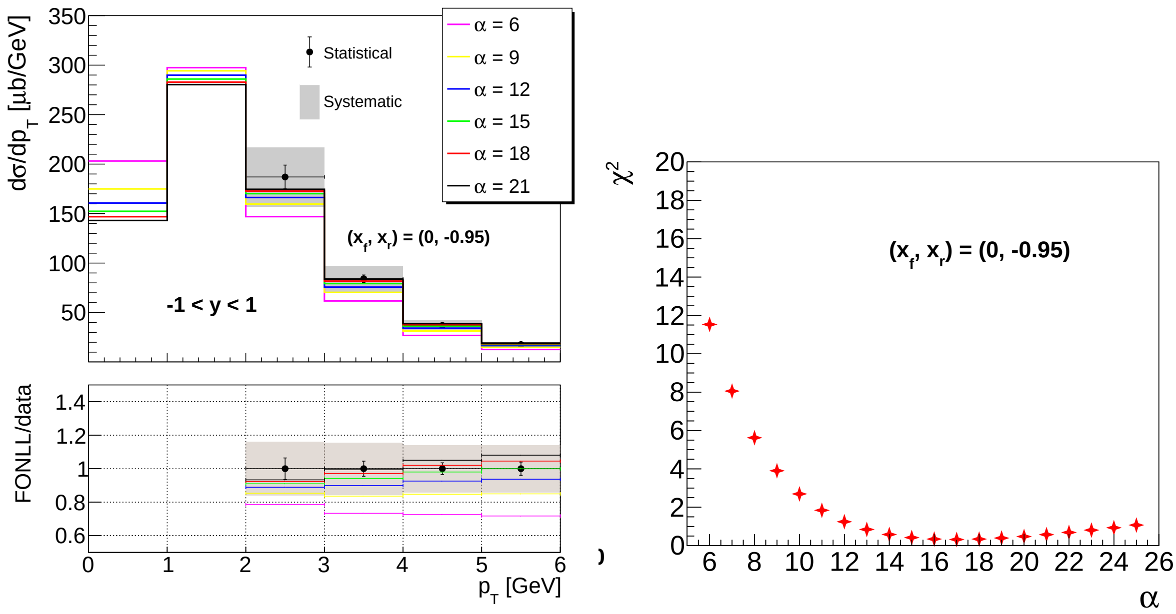

Figure 55: FONLL predictions with p_T-independent c-hadron fractions and χ^2-test values for $\frac{d\sigma}{dp_T}$ together with CMS data for different values of α.

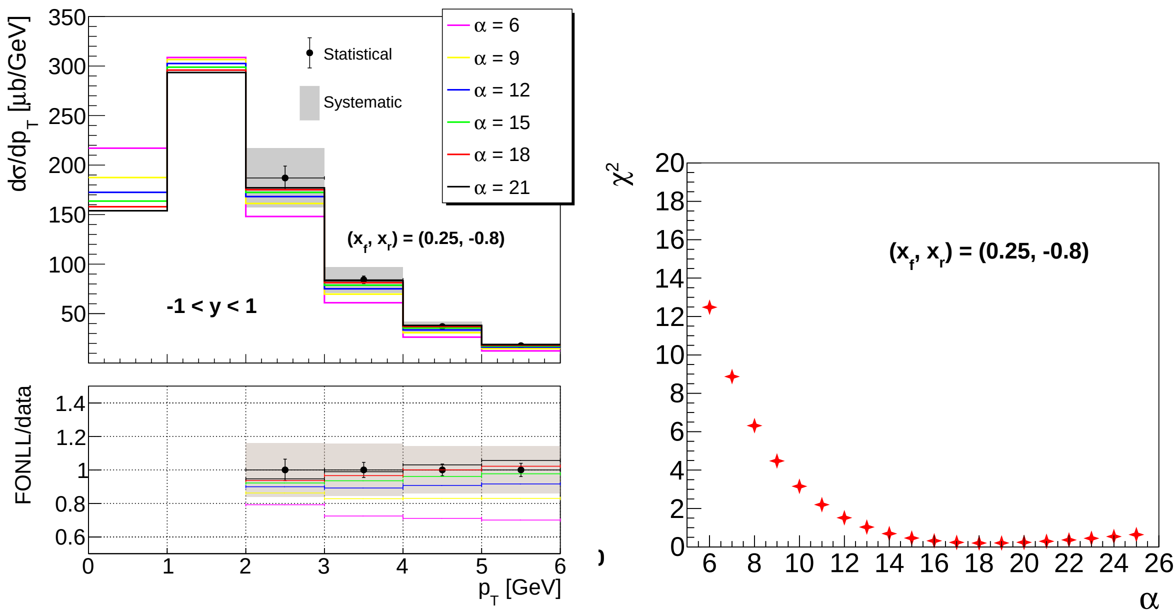

Figure 56: FONLL predictions with p_T-independent c-hadron fractions and χ^2 values for $\frac{d\sigma}{dp_T}$ together with CMS data for different values of α.

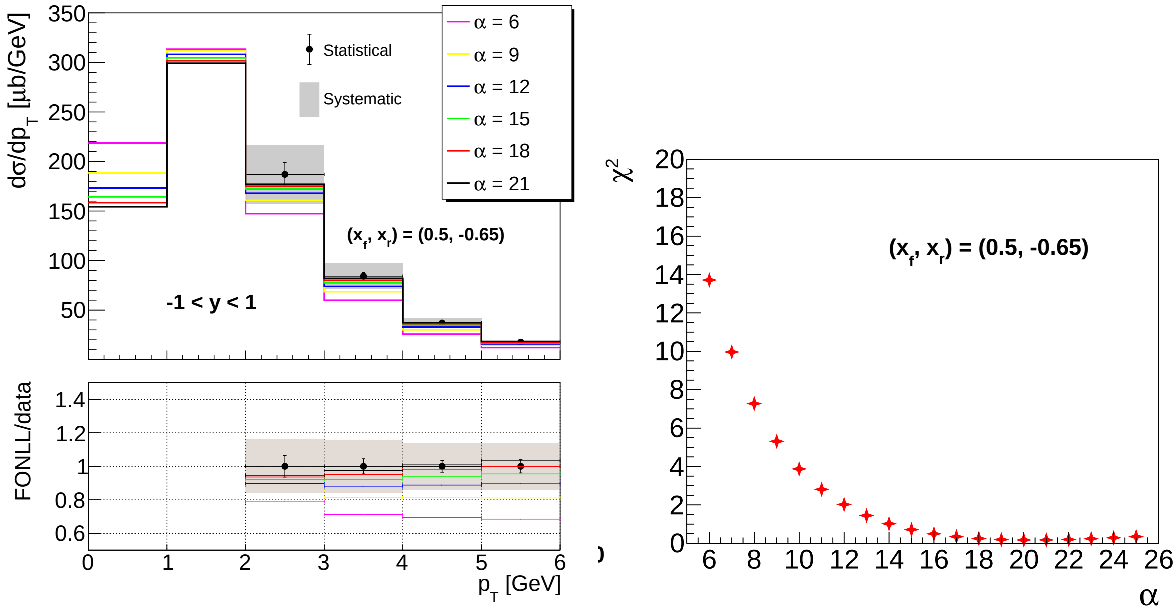

Figure 57: FONLL predictions with p_T-independent c-hadron fractions and χ^2 values for $\frac{d\sigma}{dp_T}$ together with CMS data for different values of α.

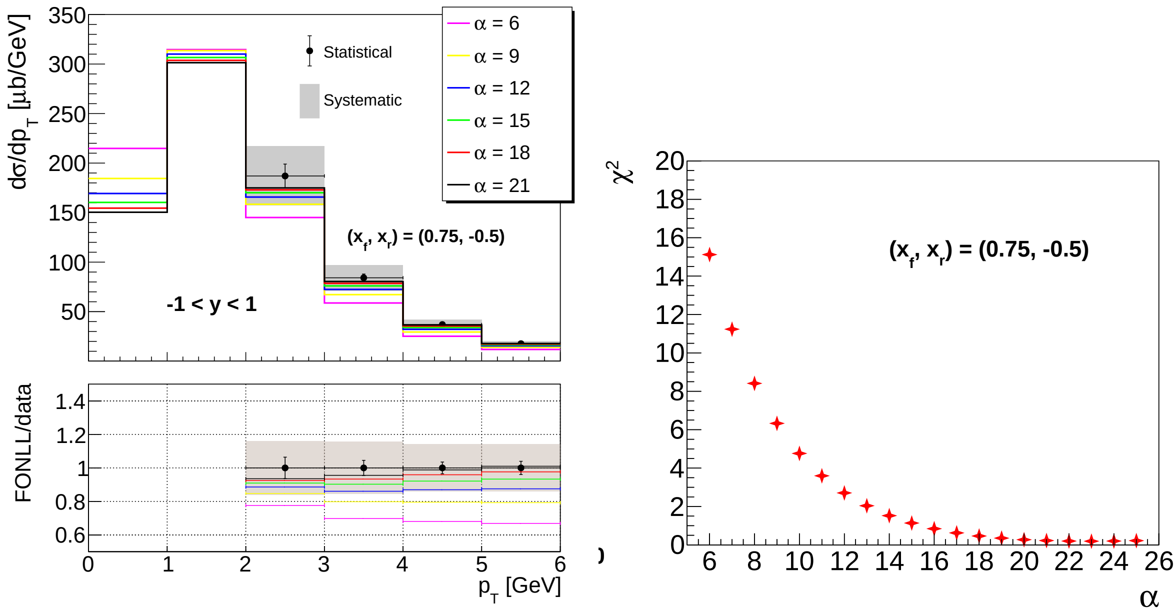

Figure 58: FONLL predictions with p_T-independent c-hadron fractions and χ^2 values for $\frac{d\sigma}{dp_T}$ together with CMS data for different values of α.

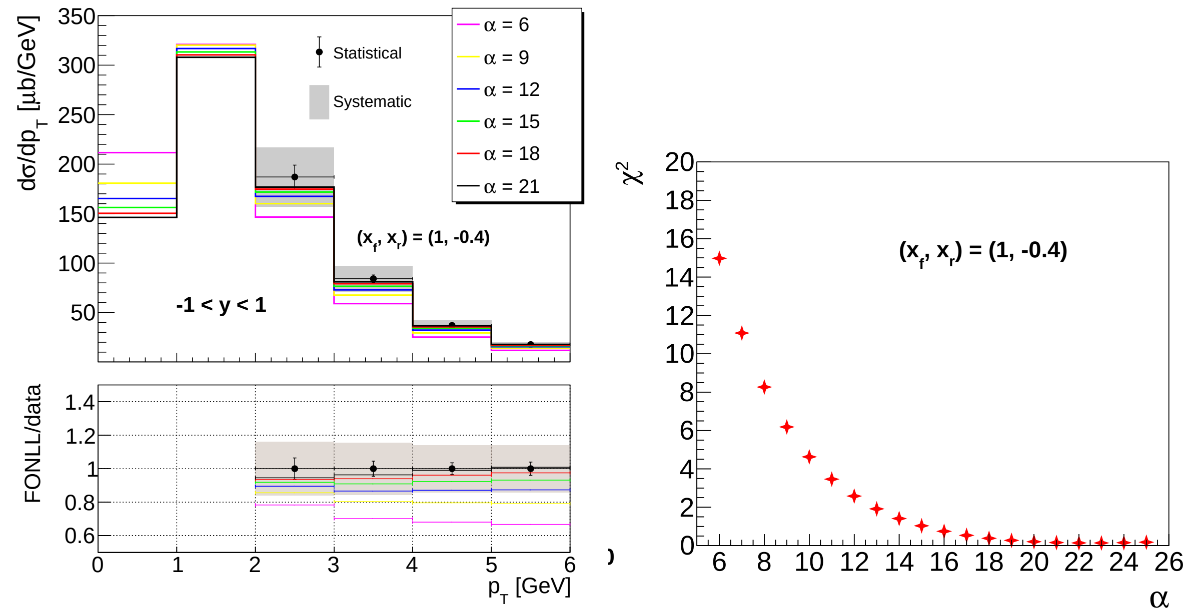

Figure 59: FONLL predictions with p_T-independent c-hadron fractions and χ^2 values for $\frac{d\sigma}{dp_T}$ together with CMS data for different values of α.

LHCb

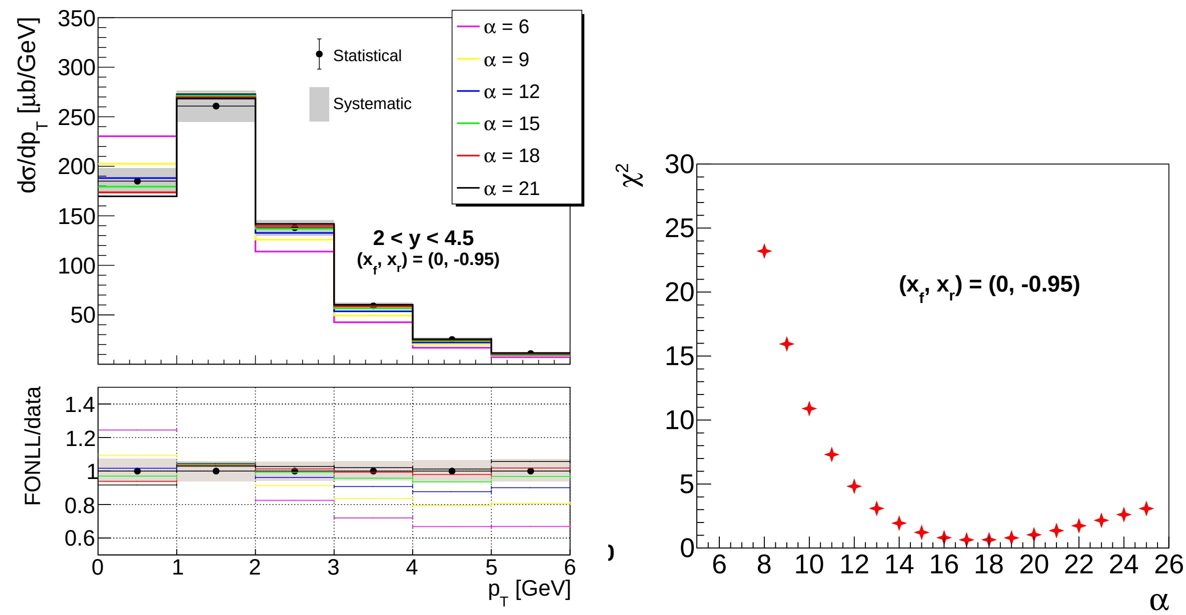

Figure 60: FONLL predictions with p_T-independent c-hadron fractions and χ^2-test values for $\frac{d\sigma}{dp_T}$ together with LHCb data for different values of α.

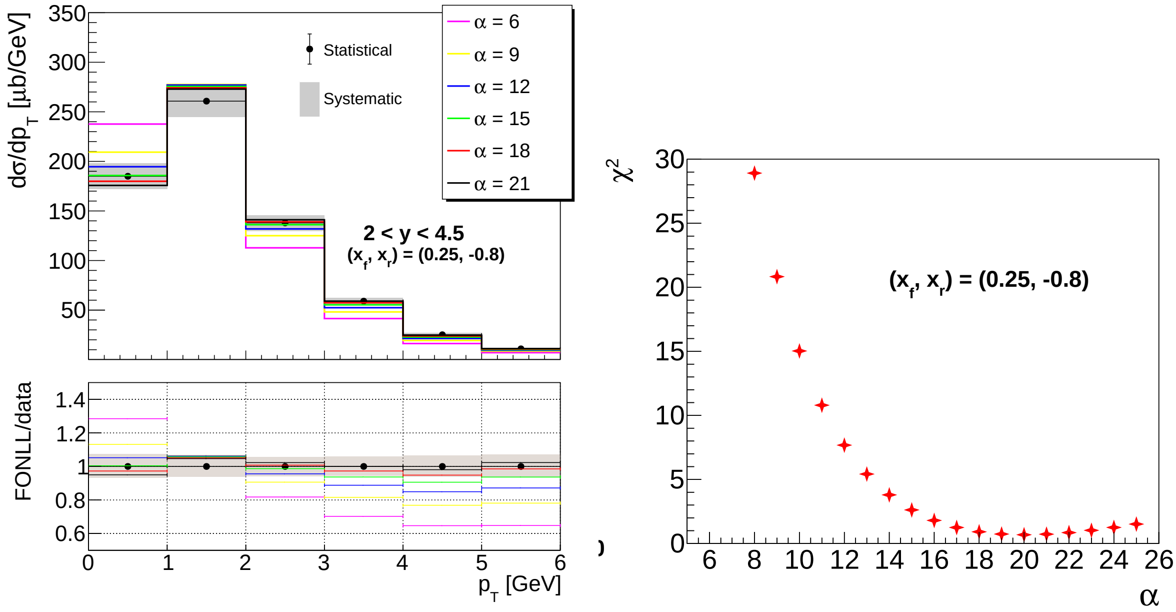

Figure 61: FONLL predictions with p_T-independent c-hadron fractions and χ^2-test values for $\frac{d\sigma}{dp_T}$ together with LHCb data for different values of α.

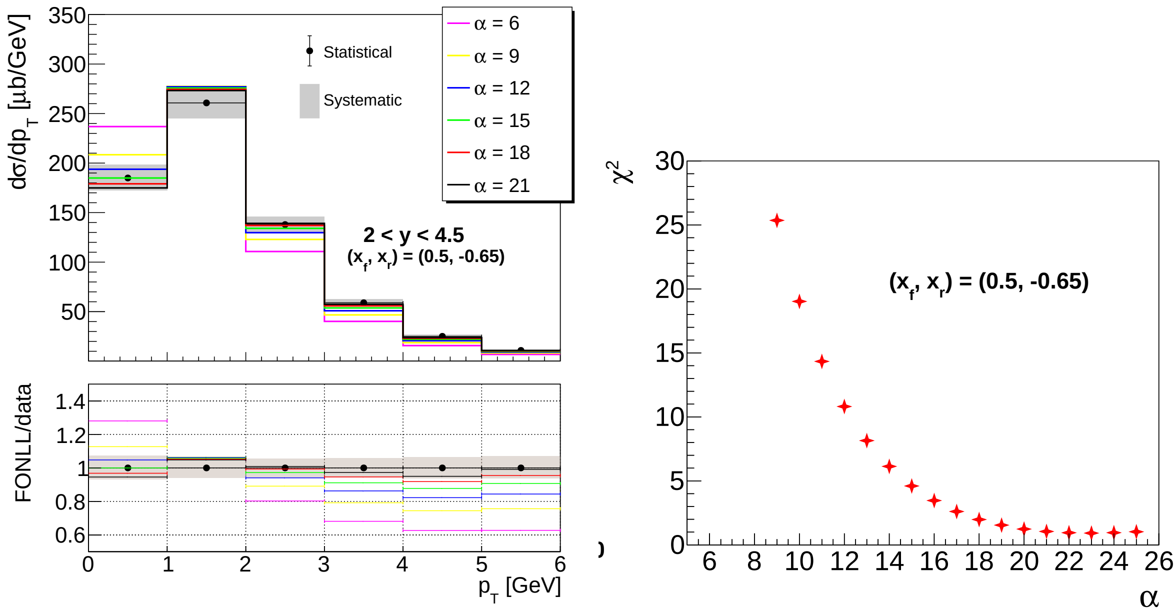

Figure 62: FONLL predictions with p_T-independent c-hadron fractions and χ^2-test values for $\frac{d\sigma}{dp_T}$ together with LHCb data for different values of α.

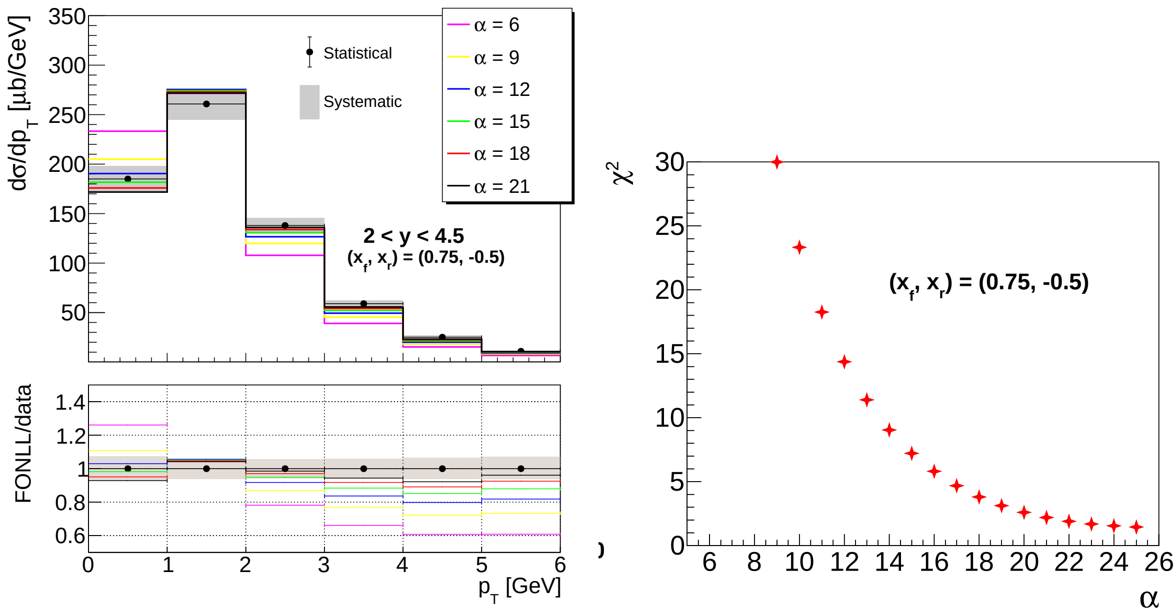

Figure 63: FONLL predictions with p_T-independent c-hadron fractions and χ^2-test values for $\frac{d\sigma}{dp_T}$ together with LHCb data for different values of α.

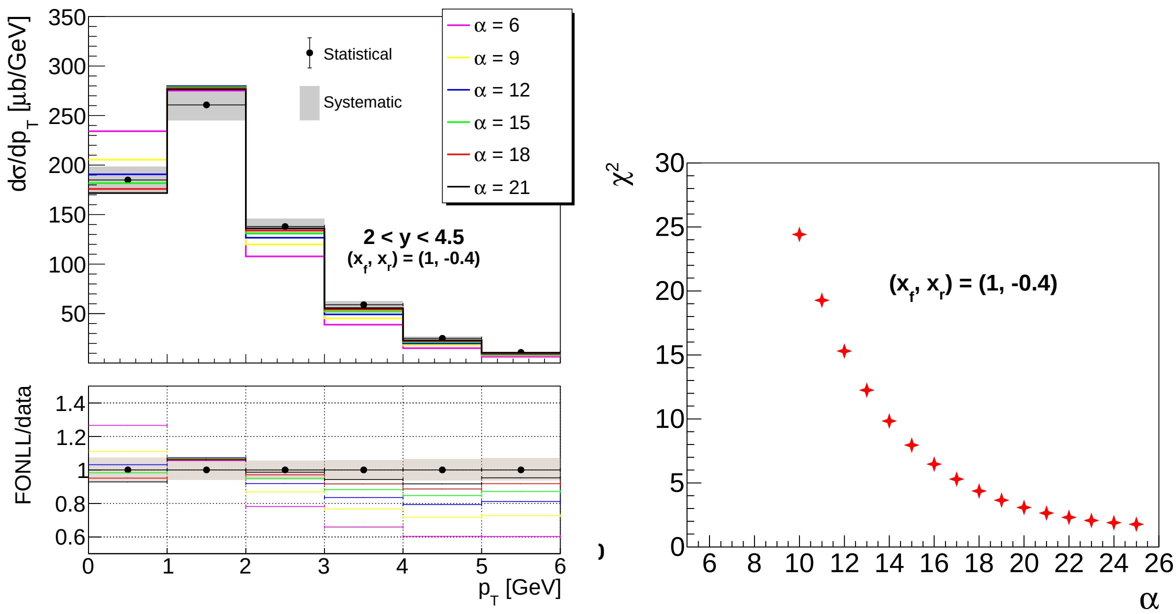

Figure 64: FONLL predictions with p_T-independent c-hadron fractions and χ^2-test values for $\frac{d\sigma}{dp_T}$ together with LHCb data for different values of α.

Combined χ^2-test values to determine the best scales

We provide combined χ^2-test values for reference and summarize the best fragmentation parameter α for every scale set in Table 8.

χ^2	Best Kartvelishvili parameter α	Scale Set (x_f, x_r)
8.51367	16	$(0, -0.95)$
7.10663	18	$(0.25, -0.8)$
7.75582	20	$(0.5, -0.65)$
9.34251	23	$(0.75, -0.5)$
10.4988	23	$(1.0, -0.4)$

Table 8: Result of the χ^2-test with $f = 21$ d.o.f. of p_T-distributions using y-integrated differential cross sections from ALICE, CMS and LHCb (see Table 1) without a p_T-dependent c-hadron fraction for D^0.

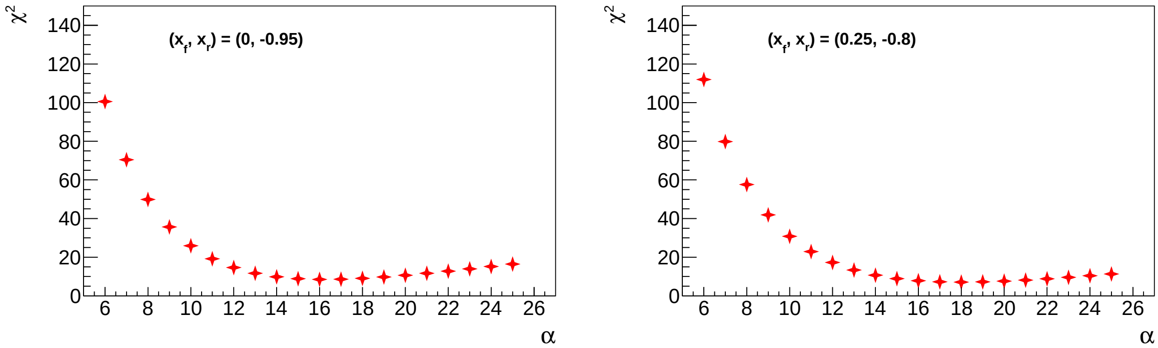

Figure 65: Combined χ^2-test values for comparing FONLL predictions to ALICE, CMS and LHCb data for 5 TeV D^0 meson production using a p_T-independent c-hadron fraction.

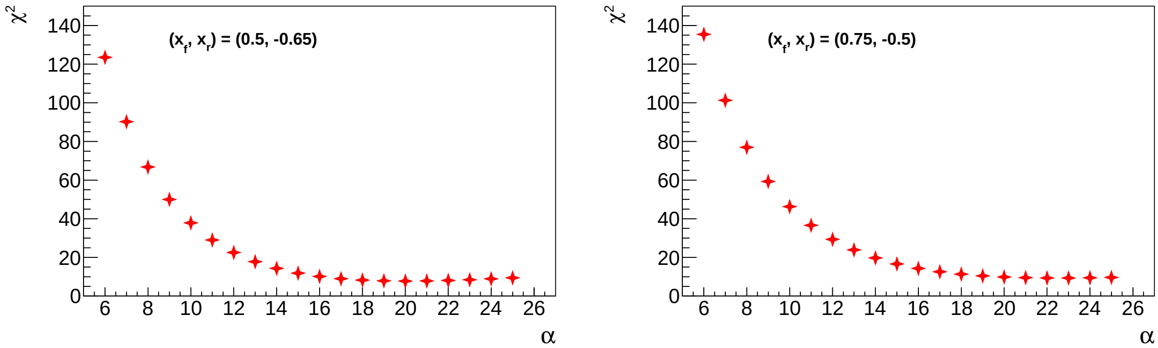

Figure 66: Combined χ^2-test values for comparing FONLL predictions to ALICE, CMS and LHCb data for 5 TeV D^0 meson production using a p_T-independent c-hadron fraction.

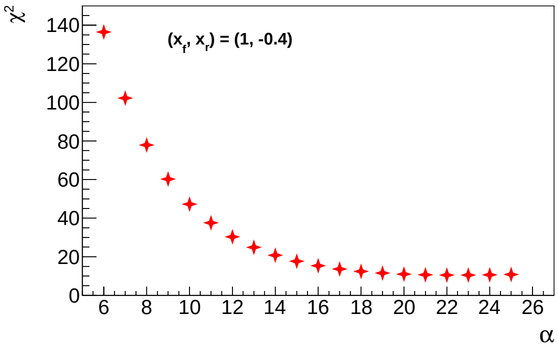

Figure 67: Combined χ^2-test values for comparing FONLL predictions to ALICE, CMS and LHCb data for 5 TeV D^0 meson production using a p_T-independent c-hadron fraction.

5.2 y-distributions for 7 TeV D^* meson production with p_T-dependent c-hadron fractions

To provide another view at the double-differential D^* meson data measured in CMS and LHCb (see Table 5), we additionally provide y-distribution plots varying x_r while keeping $x_f = 0.0$ fixed. The last bin, displayed as $4.5 < y < \infty$ denotes the y-overflow bin, covering all of the remaining phase space w.r.t. y ($y > 4.5$).

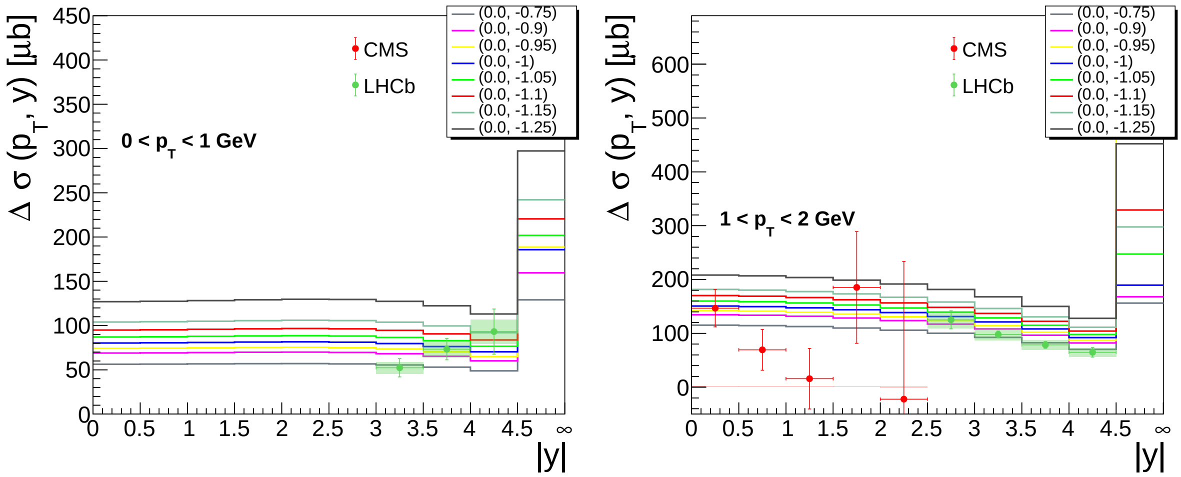

Figure 68: FONLL predictions with p_T-dependent c-hadron fractions for $\Delta\sigma(p_T, y)$ together with CMS data for different values of x_r while keeping $x_f = 0$ and $\alpha = 9$ fixed (two-tuple notation: (x_f, x_r)).

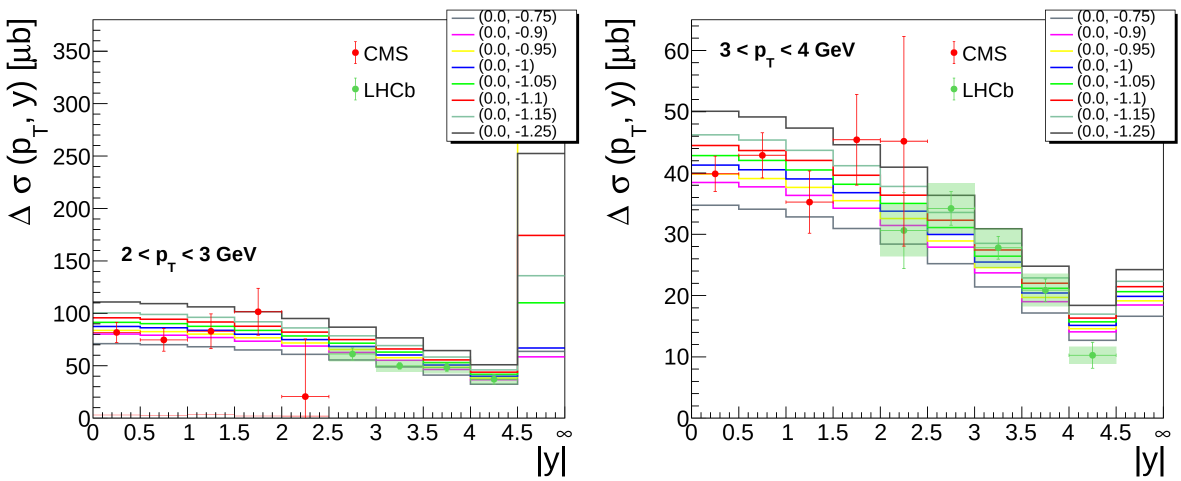

Figure 69: FONLL predictions with p_T-dependent c-hadron fractions for $\Delta\sigma(p_T, y)$ together with CMS data for different values of x_r while keeping $x_f = 0$ and $\alpha = 9$ fixed (two-tuple notation: (x_f, x_r)).

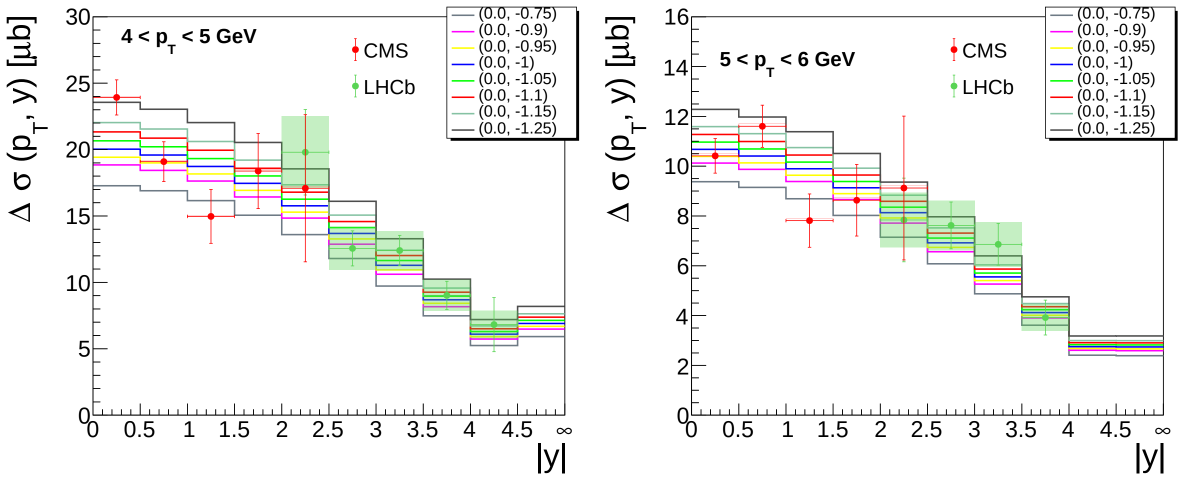

Figure 70: FONLL predictions with p_T-dependent c-hadron fractions for $\Delta\sigma(p_T, y)$ together with CMS data for different values of x_r while keeping $x_f = 0$ and $\alpha = 9$ fixed (two-tuple notation: (x_f, x_r)).

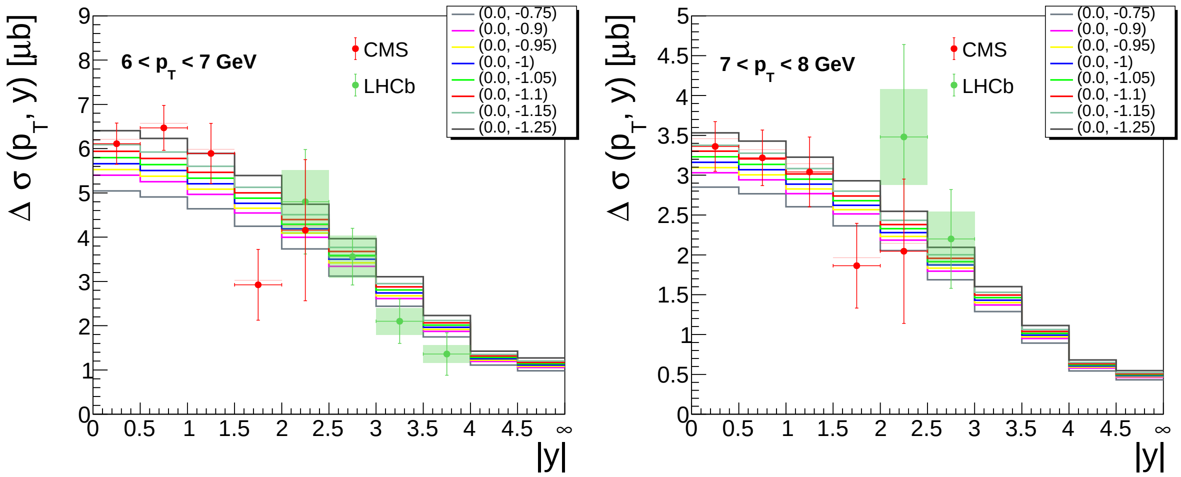

Figure 71: FONLL predictions with p_T-dependent c-hadron fractions for $\Delta\sigma(p_T, y)$ together with CMS data for different values of x_r while keeping $x_f = 0$ and $\alpha = 9$ fixed (two-tuple notation: (x_f, x_r)).

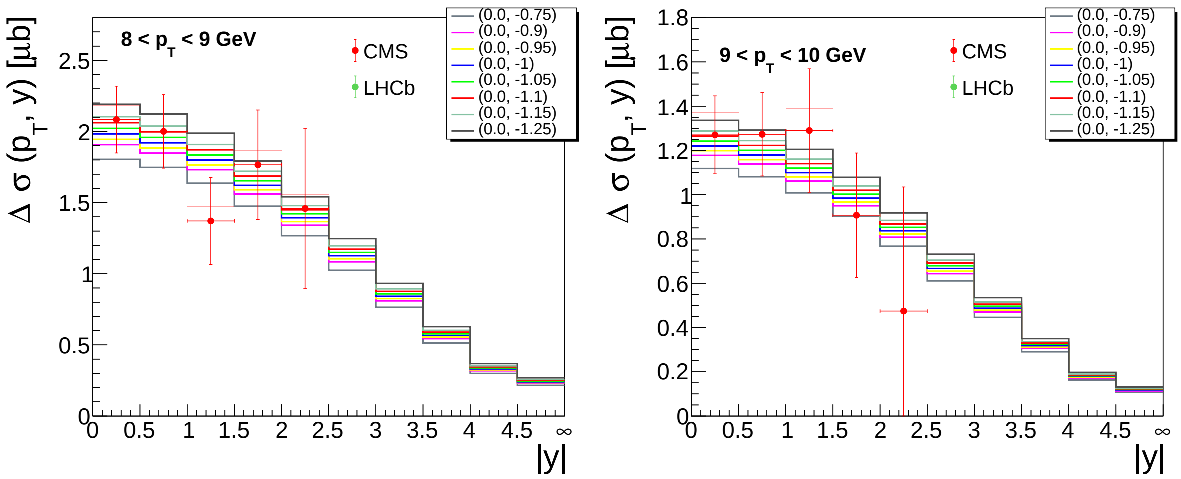

Figure 72: FONLL predictions with p_T-dependent c-hadron fractions for $\Delta\sigma(p_T, y)$ together with CMS data for different values of x_r while keeping $x_f = 0$ and $\alpha = 9$ fixed (two-tuple notation: (x_f, x_r)).

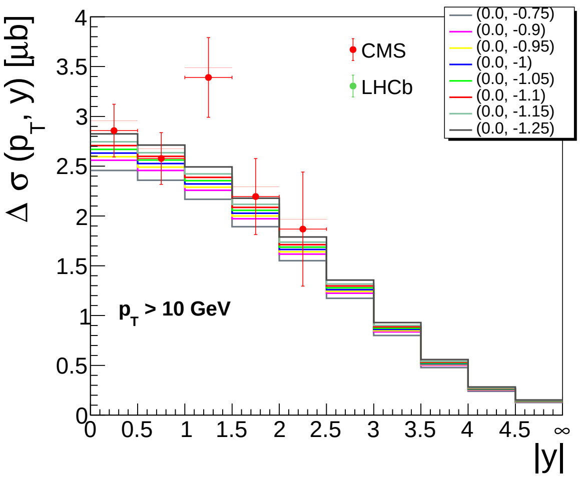

Figure 73: FONLL predictions with p_T-dependent c-hadron fractions for $\Delta\sigma(p_T, y)$ together with CMS data for different values of x_r while keeping $x_f = 0$ and $\alpha = 9$ fixed (two-tuple notation: (x_f, x_r)).

References

[1] J. C. Collins, D. E. Soper, and G. Sterman, “Factorization of hard processes in qcd,” 2004. [Online]. Available: https://arxiv.org/abs/hep-ph/0409313

[2] S. A. et. al., “Charm-quark fragmentation fractions and production cross section at midrapidity in pp collisions at the LHC,” *Physical Review D*, vol. 105, no. 1, jan 2022. [Online]. Available: https://doi.org/10.1103%2Fphysrevd.105.l011103

[3] M. Cacciari, M. Greco, and P. Nason, “The pt spectrum in heavy-flavour hadroproduction,” *Journal of High Energy Physics*, vol. 1998, no. 05, pp. 007–007, may 1998. [Online]. Available: https://doi.org/10.1088%2F1126-6708%2F1998%2F05%2F007

[4] V. Kartvelishvili, A. Likhoded, and V. Petrov, “On the fragmentation functions of heavy quarks into hadrons,” *Physics Letters B*, vol. 78, no. 5, pp. 615–617, 1978. [Online]. Available: https://www.sciencedirect.com/science/article/pii/0370269378906536

[5] K. Pearson, “X. on the criterion that a given system of deviations from the probable in the case of a correlated system of variables is such that it can be reasonably supposed to have arisen from random sampling,” *The London, Edinburgh, and Dublin Philosophical Magazine and Journal of Science*, vol. 50, no. 302, pp. 157–175, Jul. 1900. [Online]. Available: https://doi.org/10.1080/14786440009463897

[6] P. N. M. Cacciari, S. Frixione, “Fonll,” 2014. [Online]. Available: http://cacciari.web.cern.ch/cacciari/fonll/

[7] Y. Yang, A. Geiser, and J. Metwally, “Extrapolation study of total charm cross section at 5 tev with fonll,” 2021. [Online]. Available: https://indico.desy.de/event/31255/contributions/108991/attachments/68243/85803/QCD_meeting_260821.pdf

[8] M. Lisovyi, A. Verbytskyi, and O. Zenaiev, “Combined analysis of charm-quark fragmentation-fraction measurements,” *The European Physical Journal C*, vol. 76, no. 7, jul 2016. [Online]. Available: https://doi.org/10.1140%2Fepjc%2Fs10052-016-4246-y

[9] S. Acharya *et al.*, “Measurement of beauty and charm production in pp collisions at $\sqrt{s} = 5.02$ TeV via non-prompt and prompt D mesons,” *JHEP*, vol. 05, p. 220, 2021. [Online]. Available: https://doi.org/10.1007%2Fjhep05%282021%29220

[10] A. M. Sirunyan *et al.*, “Nuclear modification factor of D^0 mesons in PbPb collisions at $\sqrt{s_{\mathrm{NN}}} = 5.02$ TeV,” *Phys. Lett. B*, vol. 782, pp. 474–496, 2018. [Online]. Available: https://doi.org/10.1016%2Fj.physletb.2018.05.074

[11] R. Aaij *et al.*, “Measurements of prompt charm production cross-sections in pp collisions at $\sqrt{s} = 5$ TeV,” *JHEP*, vol. 06, p. 147, 2017. [Online]. Available: https://doi.org/10.1007%2Fjhep06%282017%29147

[12] R. A. et al., “Prompt charm production in pp collisions at sqrt(s)=7 TeV,” *Nucl. Phys. B*, vol. 871, pp. 1–20, 2013. [Online]. Available: https://doi.org/10.1016%2Fj.nuclphysb.2013.02.010

[13] O. Behnke, A. Geiser, and M. Lisovyi, “Charm, beauty and top at hera,” 2015. [Online]. Available: https://arxiv.org/abs/1506.07519

[14] M. Cacciari, P. Nason, and C. Oleari, “A study of heavy flavoured meson fragmentation functions in e+ e- annihilation,” *Journal of High Energy Physics*, vol. 2006, no. 04, pp. 006–006, apr 2006. [Online]. Available: https://doi.org/10.1088%2F1126-6708%2F2006%2F04%2F006